学位論文

Analysis of otolith formation using the medaka mutant *ha*

（メダカ突然変異体 *ha* を用いた耳石形成機構の解析）

平成 26 年 1 月 博士（理学）申請

東京大学大学院理学系研究科

生物科学専攻

北條　幹

Contents

Abbreviations

ACC: amorphous calcium carbonate

ACP: acyl carrier protein

AT: acyl transferase

BSP: bone sialoprotein

CMO: control MO

CoA: coenzyme A

cryoTEM: cryotransmission electron microscopy

DEBS: 6-deoxyerythronolide B synthase

DH: dehydratase

DIF-1: differentiation inducing factor-1

dpf: days post-fertilization

DrPKS: *Danio rerio* PKS

ENU: N-ethyl-N-nitrosourea

ER: enoyl reductase

FAS: fatty acid synthase

HGT: horizontal gene transfer

hpf: hours post-fertilization

HPLC: high-performance liquid chromatography

HpPKS: *Hemicentrotus pulcherrimus* PKS

KR: ketoreductase

KS: ketosynthase

ktu: *kintoun*

MO: molpholino antisence oligo nucleotide

MV: matrix vesicle

OlPKS: *Oryzias latipes* PKS

OmOMP-1: *Oncorhynchus mykiss* omp-1

OMP-1: otolith matrix protein-1

ORF: open reading frame

OV: otic vesicle

pks: polyketide synthase

PMC: primary mesenchyme cell

PS: phosphatidylserine

SDS-PAGE: SDS-polyacrylamide gel electrophoresis

SEM: scanning electron microscope

st.: stage

stm-l: starmaker-like

SpPKS: *Strongylocentrotus purpuratus* PKS

TE: thioesterase

TEM: transmission electron microscope

TLC: thin-layer chromatography

wt : *wild-type*

Abstract

The majority of multicellular organisms produce special minerals, biominerals, to form structures for support and protection such as bone and shell. Among biominerals, calcium carbonate is the most abundant, both in terms of the quantities produced and its widespread distribution from microorganisms to vertebrates. In spite of intensive studies, the underlying mechanism, particularly regarding the initial step of crystallization, remains a mystery. In the doctoral thesis, I addressed this question by utilizing the spontaneous medaka mutant *ha*, defective in mineralization of otoliths (ear stones) which are mainly composed of calcium carbonate.

This thesis consists of three chapters. In Chapter 1, I show that *ha* is defective in the initial step of otolith mineralization and that the causative gene is a novel medaka gene, which encodes a polyketide synthase (named OlPKS) with multi-enzyme domains. In Chapter 2, I focus on the OlPKS function in the mineraliztaion of otolith. A series of injection experiments with active site-mutated mRNAs indicates that each domain contained in OlPKS is essential and that OlPKS could function as a multifunctional enzyme. Further analyses by cell transplantation and a heterologous expression system using fungi provide an intriguing implication as to how the product of OlPKS works in the initial step of otolith mineralization. Finally, in Chapter 3, by genome database searches and drawing a phylogenetic tree I reveal that animal *pks* genes, rarely explored before my work, are

widely distributed in the animal kingdom.

My study uncovers a new link of PKS and mineralization of otolith, and further suggests the universal function of this long-neglected gene family in vertebrates in calcium carbonate mineralization.

General introduction

Biomineral

Biominerals are special minerals produced by biological activities, which give stability, rigidity, defensiveness and functionality to organisms. Physical and chemical advantage of each biomineral most probably arises from mechanisms of mineralization tightly controlled by organic materials (Addadi and Weiner, 1985; Weiner and Hood, 1975). From microorganism to vertebrate, many organisms produce various biominerals; they include magnetosome (magnetotactic bacteria, magnetite); coccolith (coccolithophore, calcium carbonate); grass opal (rice, silicate); exoskeleton (crustacean, calcium carbonate); shell (mollusk, calcium carbonate); bone and teeth (vertebrate, chalcium phosphate).

Understanding the mechanism of biomineralization has been a focus of not only biologists but also experts in other fields. How the organic components change the characteristics of biomineral (hardness, polymorph, size etc.) is a subject of great interest to mineralogists. Mechanism of calcium carbonate mineralization has attracted attention by geoscientists and paleontologist because of this mineral's role in global geochemical cycles of carbon and calcium (Van, 2003; Westbroek et al., 1993). Of course, mechanism of calcification of bone/teeth is of interest to physicians in regenerative medicine. Recently, the self-assembly nature of biomineralization process has received considerable attention from material engineers. As an example of biomimetic strategy, 'bottom-up fabrication' in which

the structure is constructed in an organized manner, is applied to nanomaterial production (Sarikaya et al., 2003).

Importance of organic matrices in the process of biomineralization

From the view point of mineralogy, there are common characteristics of the process of biomineralization. It occurs in a closed space. Organic composition of the biomineral, called organic matrix, has critical roles. Crystallization develops at near normal temperature and pressure, suggesting the presence of a precursory state (*e.g.*, amorphous phase) (Sunagawa, 2003). Generally, process of biomineral formation is divided into four steps (Fig. 1) (Lowenstam and Weiner, 1989; Sunagawa, 2003). First, the special space where mineralization occurs is formed. Next, inorganic ions are transported and concentrated there. Then inorganic nuclei are formed by organic templates, followed by the crystal growth and conformation in the context of development of the organism. These all steps are regulated by biological activities contrary to the case of inorganic mineralization. For instance, ion transporter located at the wall of the closed space keeps ion concentration high around the biomineral, that otherwise would be low concentration. More crucial and interesting biological activity is secretion of organic matrices, which regulate the mineralization process and become minor compositions of the biomineral.

Based on studies in various aquatic organisms, Nagasawa categorized organic matrices contained in the biomineral into four groups (Fig. 2A) (Nagasawa, 2013). Biominerals can be dissolved in an acidic solution and some organic matrices are concurrently dissolved in the solution. They are called water-soluble organic matrices and functionally divided into two groups (group 1 and group 2). Matrices belonging to group1 function in stabilizing and maintaining amorphous state of ions, while matrices in group 2 probably regulate the morphology and size of crystals. After decalcifying a biomineral by acidic solution, water insoluble materials remain. However, some materials can be extracted by treatment with detergent at high temperature, and they are called group 3. Organic matrices of group 3 regulate crucial features of crystal such as nucleation, orientation and crystal polymorph (*e.g.*, aragonite/calcite/vaterite in calcium carbonate). Members of group 4, called insoluble matrices, are insoluble even after detergent extraction. They act as scaffold for crystallization and they contain biopolymers such as cellulose, collagen and chitin (Fig. 2B; pink). Previously found organic matrices are listed in Table 1.

Initial step of crystallization, called nucleation, is one of the major issues in biomineralization. The formation of crystalline materials from saturated solution is classically described by the 'nucleation and growth theory', where atoms or molecules are assumed to assemble directly from solution (Kashchiev, 2000). However, recently, more

complex pathways have been proposed based on experimental and modeling studies. Using a very high resolution microscopic technique, cryotransmission electron microscopy (Cryo-TEM), the Sommerdijk group found that template-directed calcium carbonate formation starts together with the formation of prenucleation clusters, amorphous nanoparticles in solution (20 - 100 nm) (Dey et al., 2010; Gebauer et al., 2008). Although these detail observations have been performed *in vitro*, the molecular bases for regulating of these observed phenomena are largely unclear. Only a few candidates of organic matrices has been proposed to be involved in the nucleation step (Hunter and Goldberg, 1993; Inoue et al., 2007; Suzuki et al., 2009). Further experimental data are needed to explain the underlying mechanism of biomineral nucleation.

Fish otolith as a model of calcium carbonate biomineral

Most solid inorganic materials in the biota are made of calcium salts, including calcium carbonate, calcium sulfate and calcium phosphate. The use of calcium phosphate is limited mainly to the bone/teeth of vertebrate (hydroxyapatite), whereas calcium carbonate is found in various animal tissues; mollusk shell, crustacean exoskeleton, coral skeleton, coccolithphore coccolith and fish otolith.

Otolith is one of the vertebrate biominerals located within the fish inner ear and it

is primarily involved in sensing for gravity and acceleration. In teleost fish, the membranous labyrinth of the inner ear consists of the semicircular canals and the vestibular organ, filled with fluid called endolymph (Fig. 3A) (Lowenstein, 1971). The vestibular organ contains three otoliths attaching to sensory patches, called maculae, where mechanosensory hair cells are densely located. The vestibular organ is divided the three sacs: utriculus, sacculus and lagena, and each of three sacs contains an otolith called lapillus, sagitta and asteriscus, respectively. Owing to their inertial mass, otoliths can deflect the tiny sensory hair bundles of hair cells to varying extents, depending on the orientation of the vestibular organ with respect to gravity (Fig. 3B). Otolith is composed of calcium carbonate (90-98%) and a small amount of organic materices (0.2-10%) (Campana, 1999). For example, Otolin-1, a water-insoluble protein, functions as a framework of mineral deposition (Murayama et al., 2002). Starmaker is a crucial protein to determine the polymorph of calcium carbonate (otolith is normally aragonite or vaterite) (Sollner et al., 2003). Fish otolith is an attractive model of calcium carbonate biomineralization because otolith is easily to handle due to its location (near the surface of body), and each process of biomineralization can be observed in transparent fish embryos and larva.

In addition, investigation of otolith mineralization could bring some implications in the field of medical science. Although in amniote and amphibian, a group of small

particles, ‘otoconia’, with gelatinous matrix, in apparent contrast with a large dome shaped structure in teleost otolith, otolith and otoconia are thought to be functionally equivalent with orthologous structures and similar developmental mechanisms (actually most important factors are conserved between mouse and fish (Hughes et al., 2006)). In human, otoconia deficiency has been proposed to be linked to some dizziness disorder, such as menial disease and benign paroxysmal positional vertigo (Squires et al., 2004; Yamane et al., 2010). The study of fish otolith formation may help in understanding these human diseases.

Chapter 1

Analysis of the medaka mutant *ha* defective in the otolith mineralization

Introduction

Process of the otolith formation in teleost fish

Taking advantages of zebarafish system (rapid development, transparent embryos and availability of genetic techniques), many groups have investigated the process of otolith formation for the last two decades (Haddon and Lewis, 1996; Takagi and Takahashi, 1999; Whitfield et al., 1996). Mainly based on the zebrafish analyses, I summarize the processes of otolith formation (Fig. 4A): At early segmentation stages, the otic vesicle (OV), the inner ear primodium, is formed by cavitation. This vesicle consists of a single cell-layer epithelium and is filled with endolymph. Within the OV, an inorganic environment is strictly controlled, where calcium and carbonate ions are significantly concentrated, and pH is appropriately regulated for mineralization of aragonite (these biochemical data are gained using trout (Payan et al., 1997; Tohse et al., 2004; Tohse and Mugiya, 2001). Soon after the OV is formed, a large number of small particles, called seeding particles, are secreted from the OV epithelium (Clendenon et al., 2009; Riley et al., 1997). Although it is unknown whether the seeding particle contains all compositions required for otolith formation, all otolith components are thought to be supplied from the epithelium. Around late segmentation stages, the seeding particles aggregate at the anterior and posterior regions of the OV (prospective maculae) where specialized hair cell precursors, tether cells, are

located. The aggregation of particles becomes the origin of otolith mineralization, and finally two small crystals can be observed by a stereomicroscope. Among three otoliths, lapillus and saggita are crystalized at embryonic stages. Once a small crystal is formed, otolith slowly grows in its mass even in adult fish by continuously supplying the otolith components by epithelial cells. The third otolith, asteriscus, appears much later, not before 9-17 days post-fertilization (dpf), in an additional chamber, lagena.

In addition, essential roles of cilia in otolith formation have been repeatedly shown in zebrafish (Fig. 4B) (Colantonio et al., 2009; Riley et al., 1997; Stooke-Vaughan et al., 2012; Wu et al., 2011); tethering seeding particles by long kinocilia (5-8 μm) protruding from hair cells and stirring the fluid by shorter motile cilia (1.5-5 μm) lining the entire of the OV epithelium.

Medaka mutant *ha*: a gravity sensing model

One reason for our limited knowledge on the early step of mineralization is that zebrafish mutants entirely lacking otoliths have been less frequently reported than those defective in morphology, number and location of otoliths. Indeed only a few mutants or morphants are reported as ‘no otolith’ fish, but its responsible genes are not identified or, if identified, their roles are unclear (Schibler and Malicki, 2007; Whitfield et al., 1996).

Although zebrafish research has been increasingly significant in various developmental phenomena, there is an alternative choice, medaka or Japanese killifish. Biological features of medaka are mostly shared by zebrafish and there are several advantages of medaka over zebrafish; smaller genome, availability of highly polymorphic inbred strains and easiness to gain temperature-sensitive mutants (medaka is a temperate fish and can survive in a wider range of temperature). Indeed, medaka forward genetics has isolated many novel mutants with developmental defects in the last decades (Takeda and Shimada, 2010). In addition, 'Tomita Stock' provides the unique mutants (more than 90 spontaneous mutants), which were collected by late Professor Hideo Tomita at Nagoya University.

To gain molecular insight into the mechanism of the early steps of otolith formation, I analyzed a medaka mutant, *ha*, a spontaneous recessive mutant defective only in otolith and inner ear formation (Tomita, 1990). Homozygous *ha* medaka is viable and shows circular swimming behavior due to abnormal inner ear and otolith, and thus, it had been used as a model of gravity sensing (Fig. 5) (Ijiri, 2000). However, a phenotypic analysis focusing on the early otolith mineralization has not been done and the gene responsible for *ha* is not identified. In this chapter, I conduct detail phenotypic analyses and identify the causative gene using by positional cloning.

Results

Normal otolith development in medaka

First of all, I observed otolith development in wild-type (*wt*) medaka. Basically, otolith formation in medaka proceeds in a way similar to zebrafish (Riley et al., 1997). Soon after the OV is formed around st. 22 (9-somite stage), seeding particles start to float in the endolymph from st. 23 (12-somite stage) (Fig. 6A and Fig. 9) and coalesce into a small crystal at st. 24 (16-somite stage) (Fig. 8C *Upper left*). Otoliths are stereo-microscopically visible as two small crystals on both sides of an OV at st. 25 (onset of blood circulation) and continuously increase in size (Fig. 6B and 11E).

Although many studies have shown the importance of cilia function during otolith mineralization in zebrafish, this scenario may not hold true in medaka. Cilia were found on the OV epithelium of medaka, but they are much smaller in size (<1 μm) (Fig. 8A) and their motility was hard to be detected. Furthermore, probably due to their small size, I failed to identify kinocilia. Seeding particles and growing otoliths appear to be directly attached on the epithelium (Fig. 8C *Upper left*) or they might be tethered by very short cilia which are invisible by microscopy. Thus far, there is no report that described the presence of cilia in medaka OV and their function. Recent zebrafish studies show cilia are not necessary for otolith mineralization and localization (Stooke-Vaughan et al., 2012). At least, motile cilia

do not contribute to otolith formation in medaka, because the medaka mutant *kintoun* with paralyzed cilia (Omran et al., 2008) normally develops otoliths (Fig. 8C *Center*).

The *ha* embryo failed to mineralize ololiths

The gross morphology of *ha* was previously reported as significantly delayed mineralization of otoliths, slightly enlarged OVs and malformed semicircular canals (Ijiri, 2000; Mizuno and Ijiri, 2003). I further characterized the *ha* phenotypes at embryonic stages st. 22 - st. 30 (blood vessel development), when the formation of the OV and otoliths takes place.

I first analyzed the expression of molecular makers involved in early patterning of the OV and otolith formation. Around st. 22, *eya-1* was expressed entire OV region and *pax2* was expressed in medial domain of OVs. The expression of these early patterning genes were unaffected in *ha* embryo (Fig. 7 A and B). In later stages (st. 30), the expression of *dlx-3b* and *bmp-4* were restricted to the dorsal domain of the vesicles and the regions of sensory epithelium, respectively. Expression of these marker genes was comparable between *wt* and *ha* although the OV was enlarged in *ha* embryos (Fig. 7 C and D). These data suggested that OV specification and patterning were normal in *ha* embryos. In addition, organic components of otolith, such as *starmaker-like* (*stm-l*) and *sparc* were normally

expressed in *ha* OV (Fig. 7 E and F).

Acetylated-α-tubulin staining showed that short cilia were distributed in the entire OV of *wt* as well as *ha* (Fig. 8A). Further, the numbers of cilia in *wt* and *ha* OVs were investigated by counting the signals of acetylated α- and γ-tubulin (Fig. 8 A and B). There was no significant difference in the number of cilia between *wt* and mutant OVs although total number of cilia gradually increased as development proceeded. Although I was unable to evaluate the phenotype of hair cells and cilia for the above mentioned technical reason, I observed normal sensory epithelium (saccular macula) in *ha* embryos at later stages (Fig. 6D). Furthemore, in *ha* mutants, seeding particles floating in endolymph were first observed in DIC images of living embryos around st. 23 just like *wt* (time-lapse; data not shown). However, in *ha* mutants, mineralized stones never form (Fig. 6B).

Around st. 25, seeding particles floating in the endolymph and otoliths mineralized at the medial epithelium were obserbed in *wt* embryos, whereas only seeding particles were found in *ha* OVs (Fig. 6A). As development proceeded, the OV was fulfilled by numerous seeding particles and they were accumulated in the wall of the OV of *ha*. They aggregated and formed a paste-like opaque mass, instead of ellipsoidal glazed otoliths in *wt* (Fig. 6A *Right inset*). Importantly, just like seeding particles, organic materials such as OMP-1, a major soluble organic matrix protein (Murayama et al., 2004), were also secreted into the

endolymph and OMP-1-positive materials precipitate in the endolymph (Fig. 6C).

This was further supported by TEM observation; fine substances (Fig. 9; arrows), probably organic substances supplied by seeding particles (Fig. 9 D, E and J, *'s'*), accumulated around the epithelium in *ha* (Fig. 9 F - I, *Arrows*), instead of growing otoliths (Fig. 9 A – D, *Asterisks*). In *wt* OVs, fine particles were compacted into a round 'globule' as previously described by Pisam *et al.* (Pisam et al., 2002) (Fig. 9 A - D, *'g'*) and the globules then form otoliths by coalescing near the macula (Fig. 9 A - C).

From hatching stages to larval stages, the paste-like substance was compacted and consequently formed an otolith-like stone at the saccular macula of each OV in most of the mutant fries. This otolith-like stone looks like dome shape and contains OMP-1 protein, hence it appeared to be almost equal to normal saccular otolith (Fig. 7G). Some *ha* adult fish are reported to have this otolith-like structure not only at the saccular macula but also at utricular and/or lagena macula (Noro et al., 2007).

_ha_ responsible gene is a polyketide synthase

To identify the defective gene in the *ha* mutant, positional cloning was carried out by Dr. Ai Omi (a previous graduated student). As a result, the responsible region was narrowed down to 64.7 kb in linkage group 20, which harbors four open reading frames (ORFs) (Fig. 10A).

Sequencing analysis identified a 9-nucleotide deletion (3-amino acid deletion) in ORF 2 that encodes a polyketide synthase (PKS) (Fig. 10A). I thereafter named this gene as *Oryzias latipes* polyketide synthase (*olpks*). The *olpks* transcript is 6153 nt in length, comprises 6 exons and encodes a 2051 amino acid protein (Fig. 10C). PKSs are multifunctional enzymes mainly found in bacteria, fungi and plants, and catalyze the biosynthesis of a diverse group of secondary metabolite, polyketides, some of which are used for pharmaceuticals with antibiotic and mycotoxic properties (Nikolouli and Mossialos, 2012).

To verify that OlPKS is indeed responsible for the *ha* phenotype, I conducted three experiments. First, injection of an antisense morpholino-oligonucleotide (MO) designed against the first methionine resulted in effectively phenocoping *ha* (Table 2). Second, by positional cloning, I found a second mutation of OlPKS locus as another allele in *ki79* fish, which was isolated from an ENU-driven screen (unpublished; screen conducted for medaka mutants with defects in bone or blood development at the Tokyo Institute of Technology, Japan). This mutant may produce a truncated OlPKS protein in length of two-third of *wt* protein because of a nonsense mutation existing at 2499 nt the *pks* locus (Fig. 10B). The truncated OlPKS protein was not detected in epithelial cells by immunofluorescence (data not shown), probably owing to the elimination system of mis-folded proteins. Thus, *ki79* is

considered to be a null allele, though it has no phenotypic severity compared to that of *ha* allele. Third, I performed a phenotypic rescue experiments by mRNA injection. Full-length *olpks* mRNA was injected into homozygous *ha* embryos and it remarkably rescued the *ha* phenotype (Table 2).

OlPKS is expressed exclusively in the OV at the initial step of otolith formation

I performed whole-mount *in situ* hybridization of medaka *wt* embryo from st. 16 (the bud stage) to the st. 25 (onset of blood circulation). The expression of *olpks* was transient and exclusively restricted to the OV in developing embryos (Fig. 11A). *olpks* transcript was first detected in the otic placode at st. 19 (2-somite stage; Fig. 11D). At st. 21 (6-somite stage), expression was seen in the entire OV (Fig. 11 A and D). Then it was strictly confined to the medial and dorsal region of the OV epithelium around st. 22 (9-somite stage) (Fig. 11 B-D). This expression progressively decreased as the OV enlarged, eventually disappearing by st. 24 (16-somite stage), which is slightly before otoliths are visible by a stereomicroscopy (Fig. 11E).

I additionally analyzed *olpks* expressions in later stage embryo, fry and adult tissues by RT-PCR to assess whether OlPKS is involved in other biological contexts. For example, it might to be involved in the bone/teeth mineralization and the biosynthetic

pathway like FASs. However, I never could detect *olpks* expression in these samples, suggesting that OlPKS is specifically required in inner ear and/or otolith formation (Fig. 11F).

The medaka genome has three *pks* related genes including *olpks* and I named the other two genes as *olpks-2* and *olpks-3* (Table 4). The amino acid sequence of OlPKS has a similarity to the other two genes (Fig. 12). In particular, *olpks- 2* (identical to 50% of amino acids sequence) is located adjacent to the *olpks* locus, probably created by local gene duplication. I confirmed that the other two are not expressed in embryo and adult tissues by RT-PCR (Fig. 11F).

Discussion

In *ha* embryos, otolith mineralization is completely inhibited, even though major organic materials are supplied and accumulated in the endolymph. This phenotype is unique compared with those of other zebrafish mutants or morphants. For instance, MO-mediated knockdown of *starmaker* resulted in various morphological abnormalities (Sollner et al., 2003). *omp-1* morphant forms small size of otolith, while *otolin-1* morphant shows mislocalization or abnormal adhesion of two otoltihs. OMP-1 protein is a major soluble organic matrix of otolith and thought to be involved in otolith growth. Otolin-1 is a collagen

like matrix which supports the growth of otoliths and keeps otoliths on the maculae (Table 1; (Murayama et al., 2005)).

The transient expression pattern of *olpks* supports its early function and this pattern of expression also contrasts sharply with that of other essential genes identified so far. For instance, *otolin-1* and *omp-1* expression begins at st. 25 and persists into adulthood as these proteins continue to be deposited on growing otoliths throughout life (Murayama et al., 2004; Nemoto et al., 2008). Furthermore, the expression of medaka *starmaker* (called *starmaker-like*) is detected at st. 21 and is again maintained at later stages (Bajoghli et al., 2009).

Intriguingly, *ha* fry develops an otolith-like stone (Fig. 7G). This does not occur in zebrafish 'no-otolith'-type mutants such as *backstroke* and *keinstein* (Sollner et al., 2004). In both cases, secretions of the essential otolith components are perturbed, which are constitutively provided into the OV in *wt* fish (Starmaker protein and seeding particles). By comparison of these phenotypes, *olpks* gene is not likely to be involved in production and secretion of the otolith components. Rather, it probably functions as a trigger of otolith crystallization. In *ha*, continuous supply of otolith materials without initiation of crystallization could lead to abnormal development of semicircular canals and irregular stone formation at later stages.

According to Nagasawa's category (Fig. 2A), the nucleation facilitator belongs to the group 3 and it could interact with the organic matrix and inorganic ions. Thus, I next address the nature of OlPKS protein and its product to know whether OlPKS could function in the nucleation step.

Chapter2

OlPKS plays a critical role in otolith mineralization

Introduction

Polyketide synthase

The causative gene of *ha* is a novel gene belonging to the polyketide synthase (PKS) gene family. Here, I briefly summarize about this gene family. PKSs are a large family of multifunctional enzymes resembling to fatty acid synthases (FAS) (Smith and Tsai, 2007; Staunton and Weissman, 2001). PKSs catalyze the biosynthesis of polyketides, a group of secondary metabolites found in bacteria, fungi, insects and plants. Their structures are strikingly diverse, yet they share a common pattern of biosynthesis. They could include aromatic rings, lactone rings, polyethels and polyenes, and these compounds show a wide range of biological activities (Fig. 13A). Indeed, many fungal polyketides are known to be potent toxins and mutagens. Furthermore, PKSs provide a wealth of medicinally important compounds, including antibiotic, anticancer, antifungal, antiparasitic and immunosuppressive properties (Nikolouli and Mossialos, 2012).

Polyketides are produced by complex and sequential enzymatic pathways. PKSs function by carrying out Claisen-like condensations of small to long chain carboxylic acid moieties with acetate or branched chain acetate units commonly derived from malonyl-CoA or methylmalonyl-CoA. The typical reaction catalyzed by a PKS is as follows (Fig. 13B) (Hopwood, 1997). The starter unit such as acetyl-CoA is transferred to the ketosynthase

(KS) domain, and an extender unit, such as malonyl-CoA, is transferred to the acil carrier protein (ACP) by acyl transferase (AT) domain. Then, the KS domain catalyzes a decarboxylative Claisen condensation between an acyl thioester and an extender unit, resulting in the formation of a new carbon-carbon bond. The decarboxylative Claisen condensation occurs repeatedly and a polyketide chain is thus extended. In addition to this basic reaction, other enzymes, ketoreductase (KR), dehydratase (DH), and enoyl reductase (ER) are included in the system to synthesize reduced compounds. In fatty acid biosynthesis, there is a complete reduction of the keto groups with the production of completely saturated carbon chains, while these remain unreduced or partially reduced in polyketides.

Structure of PKS

PKSs are classified three groups as type I, type II and type III on the basis of gene structure (Fig. 14) (Jenke-Kodama et al., 2005). Type I PKSs are large multifunctional enzymes with multidomains necessary for polyketide assembly such as KS, AT, ACP and in some cases, KR, DH, ER, and thioesterase (TE) (Fig. 14A). In the case of type II PKSs, each catalytic site is present on a separate polypeptide and many polypeptides work together by forming non-covalent complexes (Fig. 14B). Type III PKSs form a simple structure consisting of a homodimer which performs consecutive elongation reactions at two independent active

sites (Fig. 14C). According to the gene structure, OlPKS is thought to be classified to the type I PKS group.

Type I PKS genes are further categorized into modular type (mostly in bacteria) or iterative-type ones (in fungi) (Jenke-Kodama et al., 2005). In modular PKS, enzymes consist of multiple modules and each module is responsible for one round of condensation and β-keto chain processing. Each catalytic domain of modular type I PKSs is used only once during the biosynthetic process, as exemplified by the 6-deoxyerythronolide B synthase (DEBS) for the biosynthesis of reduced polyketides such as erythromycin (Fig. 14A). By contrast, iterative type I PKSs are mainly found in fungi and composed of a single modular architecture with individual functional domains and catalyze a series of polyketide-forming reactions iteratively in a similar way to mammalian fatty acid synthases (FASs) (Fig. 14A). From the domain structure (Fig. 10C), OlPKS should belong to the iterative type I PKSs, and especially its domain organization resembles a highly reducing PKS such as the PKS involved in lovastatin biosynthesis.

Could polyketide function in animal body ?

PKS and polyketide have been traditionally and intensively investigated in microbiology as a common issue, whereas those of higher organisms tend to be neglected. Recently, an

echinoderm *pks* gene, SpPKS-1 was cloned, followed by functional assay (Calestani et al., 2003). Still, any vertebrate *pks* has never been isolated and characterized before my work.

There is little knowledge regarding the function of polyketides in developmental events, but an interesting well-known example of *Dictyostelium discoideum*. During starvation, they form multicellular structures that differentiate into a spore or stalk and, eventually, make a fruiting body. An alkylphenon, DIF-1 (differentiation inducing factor-1) synthesized by PKS critically regulates this event. I speculate that PKS functions similarly in regulating cell behavior or differentiation in vertebrates. Importantly, if polyketides are employed as signal molecules in animal development, their production and storage must be strictly controlled within a cell in terms of localization and concentration because of their strong bioactive features. For instance, they will be not accumulated in cytosol rather quickly diffuse outside of the cell. As expected, my further experiments suggest that the product of OlPKS could function in the endolymph (extracellular space). In this chapter, I focus on the nature of OlPKS and its product.

Results

All domains of OlPKS are indeed required for otolith formation

By domain search, I found that OlPKS possesses a minimal module set (KS, AT and ACP)

and additional KR and DH domains (Fig. 10C and 15A). Essential amino acid sequence motifs for the function of each domain are conserved in OlPKS (Fig. 15B). In the *ha* mutant, the amino acids corresponding to the 9-bp deletion is 'KPS', and were not previously considered as a conserved motif. However, I found that its proline is highly conserved among PKSs, and thus, I expect this residue is critical for the KS domain. Based on the structure of mammal FAS, it is likely that this proline residue helps a substrate to enter the active site of KS.

To examine whether activity of each enzymatic domain of OlPKS is required for the rescue of the phenotype, I designed five kinds of mRNA, each of which causes one amino acid mutation for enzymatic active site of KS, AT, DH, KR and an essential residue of ACP. For injection experiments, I used eggs of *ki79*, a null mutant, instead of *ha* because OlPKS protein in *ha* has intact domains except the KS domain with the 'KPS' deletion. All five mutated mRNAs were unable to rescue the *ki79* phenotype, suggesting that all domains of OlPKS were required for otolith formation (Table 3). In addition, I asked whether FAS can compensate for OlPKS by injecting of three mRNAs: full-length medaka FAS, medaka FAS lacking the TE domain-coding sequence and medaka FAS in which the KS-coding sequence was replaced by that of OlPKS (KS-swapped). These mRNAs were injected into *ki79* embryos, but the phenotype was not rescued in all injected embryos (Table 3).

OlPKS localized close to the lumen of the OV

From the results of my phenotypic analyses, I hypothesized that like other PKSs, OlPKS synthesizes polyketide-related small compounds in the OV epithelium, which facilitate the initial step of otolith mineralization.

To test this idea, I first examined subcellular localization of OlPKS using an antibody raised against an interdomain region of OlPKS. Whole-mount immunostaining revealed that OlPKS expresses exclusively in the medial wall of the OV at st. 23, which is highly localized at the apical of epithelial cells (Fig. 16 A and D) (the region for antigen is described in Fig. 16E). Double staining with an antibody to PKC ζ (Fig. 16B), an apical membrane marker, demonstrated that the distribution of OlPKS enzyme partially overlaps with that of PKC ζ but OlPKS signal is detected even closer to the lumen (Fig. 16C).

Despite its membranous localization pattern, OlPKS has no membrane-localization signal in the amino acid sequence. Thus, it may indirectly localize near the cell membrane by interactions with unknown membrane localized proteins.

Small amount of OlPKS proteins sufficiently induces otolith mineralization in a non cell-autonomous manner

To understand the property of OlPKS function in otolith mineralization, I performed a

chimaera experiment in which DsRed-expressing *wt* cells was transplanted into mutant blastula, and examined for otolith formation when *wt* donor cells colonized in the mutant OVs (Fig. 17A). I analyzed 110 OVs and assessed whether the phenotype was rescued or not, and how many and where *wt* cells were contained in the epithelium of the rescued OV.

Remarkably, irrespective of their number within the OV, *wt* cells effectively restored otolith formation at the appropriate time and location, the macula region, in *ha* embryos (Fig. 17 B - B''). In extreme cases, only a few number of *wt* cells (smaller than 10% of entire otic epithelial cells) could fully rescue the phenotype (Fig. 17 B' and D). On the other hand, otolith formation never occurred if no *wt* cell colonized in the epithelium (n=63; Fig. 17D).

Furthermore, regardless of whether *wt* cell localized at the prospective macula regions or not, otoliths were properly formed there (Fig. 17E). Even when *wt* cells colonized at the lateral wall of OV where endogenous OlPKS was not present in the *wt* embryo, otolith formation normally occurred at the right timing and in the right place, the medial side of the OV (Fig. 17B''). This shows that OlPKS protein non-cell-autonomously regulates otolith formation. It also suggests that the medially restricted expression pattern of OlPKS is not required for normal otolith formation.

As negative control, I performed a transplantation experiment in which *ha* cells

expressing DsRed were transplanted to *ha* embryos, and in these embryos, otoliths were never formed (Fig. 17C; n=19).

OlPKS actually synthesizes active compounds for otolith mineralization

I adopted a heterologous expression system to characterize substances synthesized by OlPKS (Fig. 18A). Since large-scale expression system of PKSs has been established in a filamentous fungus, *Aspergillus oryzae* (Gomi et al., 1987), I introduced the *olpks* cDNA into *A. oryzae*, expecting that exogenous PKS (*i.e.*, OlPKS) could work using endogenous substrates such as malonyl-CoA in fungal cells like their own PKSs. OlPKS expression in transformed fungi was confirmed by western-blotting in which purified OlPKS protein was investigated (Fig. 18B). Since polyketide-derivatives generally exhibit moderate hydrophobic nature, I extracted cultivated mycelia with acetone, followed by purification using partition between ethyl acetate/H_2O and subsequent purification. After concentration, residues showed no outstanding properties such as color, pH and viscosity comparing the control transformant (transformed by an empty vector). These concentrated extracts were analyzed by TLC (thin-layer chromatograph) and HPLC under various conditions, but no specific signal was detected in the sample of transformants comparing to the control transformant (data not shown).

I then attempted a simple *in vivo* assay in which *ha* mutant embryos were cultured with an aliquot of the extracts (Fig. 18A). Remarkably, these extracts could restore otolith mineralization in *ha* embryos while no such rescue was observed with control extracts (Fig. 18 C and D). Considering the simple procedure of rescue assay, concentration of the substance incorporated to the OV may not be so high. Thus, high rescue efficiency shown in Fig. 18C may suggest its high bioactivity.

These data demonstrate that it is not OlPKS but ethyl acetate extractable substances synthesized by OlPKS and secreted into the endolymph that nucleate otolith mineralization.

Discussion

A series of one amino acid mutated-mRNA injections and heterologous expression experiments strongly suggests that OlPKS functions as a type I PKS; it does synthesize active componds. However, identification of the product of OlPKS still remains elusive; I failed to detect any specific peaks in analytical experiments using extracts of *A. oryzae*, probably due to low production of the compound. To isolate of the product of OlPKS, I must establish a more efficient and stable expression system. Unfortunately, I could not predict the chemical structure of OlPKS product from the amino acid sequence of OlPKS.

In general, the prediction of the product of iterative type I PKS is difficult because the number of condensation reactions varies much, depending on a slight change in the catalytic center (probably of KS) (Cox and Simpson, 2009; Ma et al., 2009).

The cellular localization of OlPKS protein is interesting and suggestive of direct secretion of the products to the endolymph. OlPKS is likely to be indirectly anchored to the apical membrane of the epithellium in a way similar to the 'membrane-localized' PKS observed in bacterial cells. Fluorescence microscopy and TEM demonstrated that some PKSs of *B. subtilis* are assembled at a specific membrane domain (Straight et al., 2007). PpsE, a member of the Pps cluster found in *M.tuberculosis*, physically interacts with a twelve transmembrane transporter, MmpL7 using a specific interacting region. The authors suggest that the interaction with MmpL7 enables PpsE to coordinate polyketide synthesis and transport of its product destined to mycolylarabinogalactan, an extracellular structure (Jain and Cox, 2005).

If OlPKS indeed produces a polyketide or its derivatives and secrete it to the endolymph, how do they contribute to otolith mineralization ? First, the results of chimaera experiment could have some implications. Appropriate location of rescued otoliths did not depend on the location of transplanted *wt* cell. This result could exclude a possibility that PKS give a positional cue for the mineralization area like tether cells. Furthermore,

irrespective of their number within the OV, *wt* cells effectively restored otolith in *ha* embryos, which suggests that PKS does not likely belong to the molecules controlling the environment within the OV (*e.g.,* ion transporter). If these types of molecules are defective in major of epithelial cells of a chimera embryo, small amount of transplanted *wt* cells hardly compensate for the abnormality. From the same reason, it is not possible that OlPKS products are involved in growth and structural support of otolith such as OMP-1 (group 2) and Otolin-1 (group 4 in Fig. 2A). According to Nagasawa's category, the group 1 is also not likely a candidate category for OlPKS product, because its function is stabilization for ACC (amorphous calcium carbonate; the precursory state of the crystal) (Fig. 2A) (Nagasawa, 2013). Function of OlPKS may be opposite to it, as shown in phenotypic analyses.

Together with my phenotypic analyses, the results of this chapter suggest that OlPKS produce an organic matrix which functions as a 'nucleation facilitator' of otolith crystal. The nucleation facilitator is assumed to trigger or facilitate nucleus formation. Based on the function of group 3 matrices, they should contain both acidic domain and hydrophobic domain in their structure for interaction with calcium ions and structural matrices (group 4), respectively (Fig. 2A). Accordingly, my heterologous expression experiments suggest that the product of OlPKS is amphiphilic in nature, both hydrophobic

and hydrophilic like some other polyketides (*e.g.*, phenolic lipids (Kozubek and Tyman, 1999)). In my rescue experiment using the extract of *A. oryzae*, the substance dissolved in Ringer's solution could directly reach inside the OV through the epidermis of embryos and epithelial layers (Fig. 18A). The amphiphilic nature is supported by the following facts. In the processes of rough purification (see materials and methods), when the mycelium extract was partitioned between ethyl acetate/H_2O, active compound moved into the ethyl acetate phase (judged by the medaka rescue assay; data not shown), suggesting their hydrophobic nature. By contrast, when the extract was partitioned between hexane/90%MeOH, active substances existed in 90%MeOH phase (data not shown), suggesting their hydrophilic nature. Together, the amphiphilic product could serve as a bridge between calcium ion and/or ACC and insoluble scaffold matrices (*e.g.*, Otolin-1) (Murayama et al., 2002). Supporting this idea, in studies of High-resolution Cryo-TEM imaging, monolayers of fatty acids (arachidic acid or stearic acid) that are also amphiphilic in nature, have been used to artificially facilitate crystal nucleation (Dey et al., 2010; Pouget et al., 2009).

Chapter 3

Broad distribution of *pks* genes in the animal kingdom

Introduction

Presence of *pks* genes in animal genomes.

The increasing availability of whole-genome sequence information from various species has driven phylogenetic analyses for type I *pks* genes and these results show that they are more universally distributed in the phylogenetic tree than previously considered (Foerstner et al., 2008). Furthermore, many *pks* genes identified in new genome database could be candidates for 'combinatorial biosynthesis', an approach in which genes from different organisms are assembled to design and construct an artificial gene cluster for production of useful bioactive compounds as well as biofuels (Horinouchi, 2009).

Previous phylogenetic analyses also demonstrated the presence of fish, bird, sea urchin and nematode *pks* genes (Castoe et al., 2007; Leibundgut et al., 2008; O'Brien et al., 2014), but none of them were cloned and characterized except for two echinoderm genes, *pks-1* and *pks-2* (isolated from *Strongylocentrotus purpuratus*) (see below). In this study, I, for the first time, isolated and characterized the vertebrate PKS genes. This prompted me to investigate other type I *pks* genes in the animal kingdom using updated genome data sets.

Echinoderm *pks* genes

A sea urchin gene, *pks-1* was cloned from a differential screening for secondary

mesenchyme specific genes (Calestani et al., 2003). It is expressed exclusively in the pigment cell and contributes to the biosynthesis of a polyketide compound, naphthoquinone for pigment echinochrome A (Ageenko et al., 2011). Currently, the function of sea urchin echinochrome is not completely understood, but may include roles in immuno-defense (Service and Wardlaw, 1984). Considering known bacterial and fungal PKS function, this scenario is not surprising.

On the other hand, *pks-2* gene is expressed in primary mesenchyme cells (PMCs) that give rise to spicules, larval skeletons made of calcium carbonate (Beeble and Calestani, 2012). Its expression pattern is restricted in the onset of mineralization. Intriguingly, *pks-2* was included in the gene regulatory network of skeletal morphogenesis, and placed immediately downstream of Ets and Alx1 (transcription factors) which constitutes the earliest inputs into the network (Rafiq et al., 2012). These data strongly suggest a possibility of conserved roles of PKSs in calcium carbonate mineralization between medaka and sea urchin. During this study, my collaborators and I analyzed the *pks-2* gene in *Hemicentrotus pulcherrimus*.

Results

pks genes are distributed throughout animals

I performed thorough database searches for animal type I *pks* genes. Identified *pks* gene candidates were then assessed for domain structure in each predicted amino acid sequence. Here, I defined a gene containing the basic domain KS and AT, and other additional domains, as a type I PKS. These searches revealed a remarkably broad distribution of *pks* genes from Cnidaria to Bilateria, including coral (*Acropora digitifera*), turtle and marsupialia (Fig. 19A and Table 4). Usually, 1-3 *pks* genes are present in each genome, except for the lancelet genome that contains 13 genes. Most vertebrate PKSs have 5 domains which are similar to OlPKS (*e.g.*, KS, AT, DH, KR and ACP; Table 4). By contrast, some other animal PKSs are not similar to OlPKS and have versatile domains; especially *C. elegans* PKS contains 21 domains in the polypeptide (predicted by Pfam search) (O'Brien et al., 2014).

Medaka genome harbors two other putative paralogous genes as described in Chapter 1 (Table 4), whereas zebrafish has two candidates *wu:fc01d11*(XP_682975), and *si:dkey-61p9.11* (NP_001041530) (Table 4). Whole-mount *in situ* hybridization experiment demonstrated one of them, *wu:fc01d11* (named zebrafish PKS; DrPKS) was expressed in OV during segmentation stage embryo (Fig. 19B), suggesting the conservation of PKS function in teleost fish. Unfortunately, knockdown experiments in zebrafish embryo by two types of MOs targeting for *drpks* (first-Met MO and exon-intron boundary MO) failed to

reproduce the otoltih phenotype of *ha*. It is probably due to compensation by unknown paralogues. In addition, the expression of candidate of a chick *pks* candidate (XP_418588; Table 4) was not evident from RT-PCR and *in situ* hybridization at segmentation stages (data not shown).

Phylogenetic tree of animal polyketide synthases

A core motif among PKS proteins includes the typically adjacent KS and AT domains, and these domains represent the most conserved regions among PKSs. Because the structure of type I PKS is complex and includes interdomains with various lengths, phylogenetic analyses are usually conducted using this core motif or solely using the AT or KS domain (Castoe et al., 2007). Here, maximum parsimony phylogenetic analysis was conducted using the sequence of KS domain. To know the phylogenetic relationship animal *pks* genes with other known genes, I used the sequences of all animal *pks* genes in Table 4 and some genes of bacteria, fungi and protozoan which were harvested by BLAST search for OlPKS.

The phylogenetic tree demonstrates a clear discrimination of animal PKSs from the animal FAS clade (Fig. 20). Although grouping of animal PKSs encounters difficulties evidenced by low bootstrap values, they likely fall into three clades, one major and two minor (Fig. 20). The major clade (animal PKS Clade I) encompasses nearly all animal

groups, while the two sea urchin genes, *sppks-1* and *sppks-2* are classified into distinct clades together with some of the lancelet *pks* genes, animal PKS Clade II and Clade III, respectively (Fig. 20).

An echinoderm *pks* gene, *hppks-2* is essential for mineralization of the spicule

I hypothesized that like medaka PKS, some of the other animal PKSs participate in biomineralization, more specifically calcium carbonate mineralization. In this context, echinoderm *pks-2* is important, because it is likely involved in spicule formation. My collaborator, Dr. Mariko Kondo, confirmed the PMC-specific expression of *pks-2* (*hppks-2*) in our experimental system, the sea urchin, *Hemicentrotus pulcherrimus*. The expression pattern of *hppks-2* is restricted in the PMCs, which is similar to *sppks-2* (Beeble and Calestani, 2012). Importantly, the expression of *hppks-2* disappears around late gastrula stage just after PMCs begin to form spicules (Fig. 21A, *Lower Panel*). Then, Dr. Gen Hamanaka, examined the function of HpPKS-2 by injecting of first Met-MO. As shown in Fig. 20B, HpPKS-2 morphants exhibited severe defects in spicule formation, while control 5-mispair MO-injected embryos appeared normal (Fig. 21B, *Right*). Another echinoderm *pks* gene, *hppks-1* was found to contribute to pigmentation as previously reported (Fig. 21A *Upper Panel* and B, *Left*) (Calestani et al., 2003).

Discussion

I found possible orthologues of OlPKS in bird, reptile, teleost fish, amphioxus and marsupial. Thanks to recently available data such as turtle and coral, I made a more feasible blue print of the distribution of *pks* genes in the animal kingdom.

However, it is still difficult to explain the reasons of gaining and losing of these animal *pks* genes during animal evolution (Fig. 19A). For instance, if I implicate the *pks* gene in the mineralization of ear stone, otolith (not otoconia), there are some inconsistencies. Why do only reptile/bird have *pks* genes despite all amniotes equally have otoconia? Why does marsupial have *pks*? (monotreme candidate gene may be a pseudogene). Among primitive chordates (lancelet, ascidian larva and lamprey), the presence of *pks* is also not consistent, although there are not sufficient information about their statolith (sensory organ for gravity and balance). Of course, these discrepancies are partially originated from incomplete genome information. Anyway, I should interpret the roles of animal *pks* gene with a wider viewpoint (*e.g.*, calcium mineralization) and more experimental data of animal *pks* are strongly needed. I will discuss this point later.

The phylogenetic analysis based on the KS domain demonstrates the topology in which animal PKSs are separated from the animal FAS clade. Unlike the *fas* genes, the distribution of *pks* genes in animals is irregular; they are not found in some animal groups,

for examples, fly, frog and mammals, most intensively studied model animals (Fig. 19A). These facts complicate the evolutionary origin of animal *pks* genes, while a single origin of animal *fas* has been repeatedly supported. Horizontal gene transfer (HGT) could account for this mystery. Intriguingly, some bacterial type I PKSs (*e.g., Mycobacterium smegmatis*, *Paenibacillus mucilaginosus* and *Saccharothrix espanaensis*), related to the animal PKS and FAS (Fig. 19A; Table 4), possess a multidomain architecture similar to animal PKSs (KS-AT-DH-KR-ACP). It is therefore likely that multiple gene losses, gene duplications as well as HGT have contributed to the evolution of type I PKS in the animal lineage. A similar scenario was reported in bacterial/fungal PKSs (Foerstner et al., 2008; Jenke-Kodama et al., 2005; John et al., 2008).

From our analyses in *H. pulcherrimus*, I conclude that echinoderm *pks-2* plays a critical role in the formation of calcareous skeletal elements in larva. This result demonstrated a conserved role of PKS in calcium carbonate mineralization among animals. Unfortunately, I failed to isolate or detect the avian *pks* candidate during the inner ear development stage, but, I now realize that all calcareous tissues in addition to otolith/otoconia need to be investigated as target organs. The expression of other unknown animal *pks* genes might be restricted spatiotemporally as in the cases of *olpks* and *hppks-2*, thus their expression analyses should be more carefully and thoroughly conducted.

Despite their conserved roles in calcium carbonate minelalization, the product of HpPKS-2 may not be identical to that of OlPKS because the domain architecture of sea urchin PKS-2 differs to some degree from that of OlPKS, being KS-AT-DH-ER-KR-ACP-TE and KS-AT-DH-KR-ACP, respectively (Beeble and Calestani, 2012) (Table 4). In general, the amino acid sequences of organic matrices are not well conserved between species although they commonly have highly acidic regions such as Asp rich domains (Addadi and Weiner, 1985; Weiner and Addadi, 1991). Thus, a difference of chemical structure between PKS product of sea urchin and that of medaka may not be critical one. However, the presence of thioesterase (TE) in the sequence of sea urchin PKS-2 is important when we consider the enzymatic pathway and speculation of the product of the PKS. The TE domain, usually located at the C-terminal end, catalyzes the final step to release products from the PKS enzymes by a Claisen cyclization of the polyketide intermediates, leading to C-C bond formation, accompanied by cleavage of the thioester bond between ACP and the polyketide intermediate. OlPKS without TE domain may release a product by another releasing enzyme such as β-lactamase (Awakawa et al., 2009; Fujii et al., 2001). If OlPKS indeed requires another enzyme to release the product, the results of heterologous expression experiment imply that some fungal (endogenous) enzymes might help the release of OlPKS product. It is possible that the compensation by

some fungal endogenous enzyme was not sufficient to yield the OlPKS product. Therefore, I consider that sea urchin PKS-2 containing TE domain is more suitable to isolate the product of PKS in the heterologous expression system. A heterologous expression using HpPKS-2 and an injection of *hppks-2* mRNA into the mutant fish are intriguing experiments to understand the functional conservation of sea urchin and medaka PKSs. Future analytical chemistry and enzymological studies about HpPKS-2 and OlPKS should yield valuable clues for understanding a common mechanism of spicle, otolith and other calcium-based biominerals.

General discussion

Potential analogy between bone and otolith

For decades, the mechanism of bone mineralization has been investigated and the role of nucleation facilitator has been discussed. Because many similarities in the mechanism of otolith and bone mineralization were recently reported (Hughes et al., 2006), I could obtain helpful insights from bone mineralization. In the OV, seeding particles secreted from the epithelium are aggregated with collagen-like materials such as Otolin-1. Likewise, in bone mineralization tissues, ‘matrix vesicles’ (MVs) secreted from osteoblast or osteoclast are observed in the meshwork mainly composed by type I collagen, and they become start sites of deposition of hydroxyapatite crystal (Anderson, 1969) (Fig. 22A). In particular, it is interesting that acidic phospholipids such as phosphatidylserine and phosphatidylinositol enriched in the membrane of MV play a crucial role in the nucleation (Wuthier, 1975). Phosphatidylserine (PS) has especially high affinity to calcium ions, leading to the formation of a complex, calcium-phosphate-lipid complex (Boskey and Posner, 1977) (Fig. 22B). Furthermore, it was reported that phospholipid induce the hyroxyapatite mineralization in a steady-state crystallization experiment like bone sialoprotein (BSP) (Boskey, 1989). Recently, the possibility of PS and PS-mimickng coating vesicle to promote the calcification in medical implant has been investigated (Merolli et al., 2006; Satsangi et al., 2003).

These physiological and molecular analogies with bone mineralization support the hypothesis I proposed in Chapter 2: the product of OlPKS functions as a nucleation facilitator. Perhaps, OlPKS products, polyketides or its derivatives, are not directly provided into the OV, but attached with the membrane of seeding particles just like acidic phospholipid included in the membrane of MV (Fig. 22C). Further, resemblance between sea urchin spicule and vertebrate bone was evidenced by the observation of special granules at nucleation sites of PMC and finding a number of organic materials such as annexin and some glycoproteins (Beniash et al., 1999; Mann et al., 2010). The present data about OlPKS and HpPKS-2 could provide implications for understanding some common mechanisms of biominerals found in higher animals.

Future works to demonstrate the nucleating function

Here, I discuss what experimental data are needed to prove that OlPKS product indeed serve as a nucleation facilitator.

First of all, it is required to purify and analyze its chemical structure. To isolate the product of OlPKS, we must establish a more stable expression system than this study (identification of the HpPKS-2 product is an alternative choice as discussed in Chapter 3). Previous studies show that the nucleation facilitator contains two regions in their structure:

the structural matrices binding domain and crystal binding domain (acidic domain). Indeed, nucleation facilitators or other group 3 matrices (listed in Table 1) were originally isolated as acidic proteins or peptides which can interact with calcium ion. For instance, CAP-1, a peptide isolated from crayfish exoskeleton, contains a chitin binding region and an acidic region (1 Glu, 6 Asp and 1 Phospholylated-Ser) (Inoue et al., 2007). As described in Chaprer2, if the product of OlPKS is polyketide or its derivative, it should include these two regions.

Next, a kind of *in vitro* induction experiment will be necessary for demonstration of the function. BSP is as an acidic sialoprotein, traditionally studied as a nucleation of hydroxyapatite. It is capable of promoting hydroxyapatite nucleation in a steady-state agarose gel system in which Ca^{2+} and PO_4^- ions are contentiously supplied (Hunter and Goldberg, 1993). BSP is first demonstrated as a bone crystallization inducer. In addition, functions of other nucleation facilitators, CAP-1 in crayfish exoskeleton and Pif in oyster pearl, were also evident from *in vitro* experiments (Inoue et al., 2007; Suzuki et al., 2009). Regarding the otolith, an *in vitro* aragonite crystallization experiments was already reported (Tohse et al., 2009). In future, this type of induction experiments should be performed using purified OlPKS product.

Finally, localization of the product will provide important evidence. For example,

BSP transcripts are expressed at a high level in areas of *de novo* bone formation during the early phase of hydroxyapatite deposition (Chen et al., 1996; Kasugai et al., 1992). Immunohistochemical SEM images show that Pif protein is densely located at a place for the initiation of pearl crystallization, called the organic boundary between the nacreous and the prismatic layers (Fig. 23A arrow) (Suzuki et al., 2009). Intriguingly, gold particles are also found in each compartment of the entire shell layer less densely than in the boundary (Fig. 23A). As shown in Fig. 2, biominerals increase their mass by alternatively stacking the crystal layer and the matrix layer containing structural (scaffold) matrix (chitin in case of the pearl). The distribution of Pif indicates persistent requirement for subsequent stacking of aragonite tablets in the nacreous layer. Given that the otolith growth persists to adult, it is difficult to postulate that OlPKS is responsible for the 'later' nucleation of each crystal layer. Rather, it may contribute to only 'initial' nucleation at the onset of otolith formation. In zebrafish, a TEM observation combined special staining method revealed that some granular glycogen spots were observed in very early mineralization stages and a condensed glycogen signal was located at the center of growing otolith crystal (Fig. 23B) (Pisam et al., 2002). In addition, a number of polysaccharides, N-acetyl glucosamine, N-acetyl galactosamine and mannose, are contained in otolith matrix, and their carboxyl groups could bind calcium ions (Borelli et al., 2001; Hunter et al., 1988). How these

polysaccharides contribute to otolith nucleation is still unknown. Possibly, the product of OlPKS could participate in the initial nucleation, together with these organic materials (Fig. 22C). Identification of the chemical structure of the product will enable us to analyze the localization of the product using some labeling methods.

Implications of widespread distribution of *pks* genes in animal genomes: a hint to the carbon cycle on earth.

Sea urchin *pks-2* could be functionally equivalent to *olpks* because of its early and transient expression in the calcifying cell lineage and the phenotype of MO-injected embryos. Thus, it is likeky that calcium carbonate biomineralization generally requires the products of PKSs for nucleation. For instance, *pks* genes of bird and reptile might be involved in production of egg shells. In frogs and mammals, however, *pks* genes were no longer needed and lost during evolution, although their inner ears still contain calcium carbonate biominerals. Further intense search in those vertebrates which appear to have lost *pks* genes will definitely be needed.

Although highly speculative, PKSs could participate in the production of coral skeletons and calcification of algae in the ocean. For instance, a kind of sea algae, *Emiliania huxleyi*, which produces coccolith (calcium carbonate) and largely contributes to fixation of

carbon dioxide (John et al., 2008; Jones et al., 2011), has some *pks* genes (e.g., *fgeneshEH_pg.50__74*, protein ID103465, Joint Genome Institute (http://jgi.doe.gov/)). The presence of PKS in Cnidaria appears to be associated with biomineraliztion. Coral (*A. digitifera*) has a couple of *pks* genes, whereas other animals with no calcareous tissues, hydra (*Hydra magnipapillata*) and sea anemone (*Nematostella vectensis*) do not (Fig. 19A).

Furthermore, recent metagenome analyses show that sponge symbionts have various *pks* genes, including novel group of type I *pks* (Della Sala et al., 2013). Thus far, a number of species belonging to Class Demospongiae (major type of sponge) are analyzed. It will be interesting to ask whether the calcareous sponges (Class Calcarea) also have these special symbionts and PKS contribute to the calcium carbonate mineralization of the host.

Conclusions

Starting with the medaka mutant with otolith formation defects, I came up with the novel role of PKS in the onset of mineralization. This is the first report that isolates vertebrate *pks* gene and addresses its function. The generality of this novel PKS function is further supported by the recent data of sea urchin HpPKS-2, together with my phylogenetic study that identifies PKSs in a much wider range of animals than previously estimated. My finding also provides genetic and molecular cues for the geochemical study of global carbon and calcium cycles. Further functional analyses of newly identified PKSs will uncover a long-overlooked world of polyketides and their derivatives in animals.

Figures

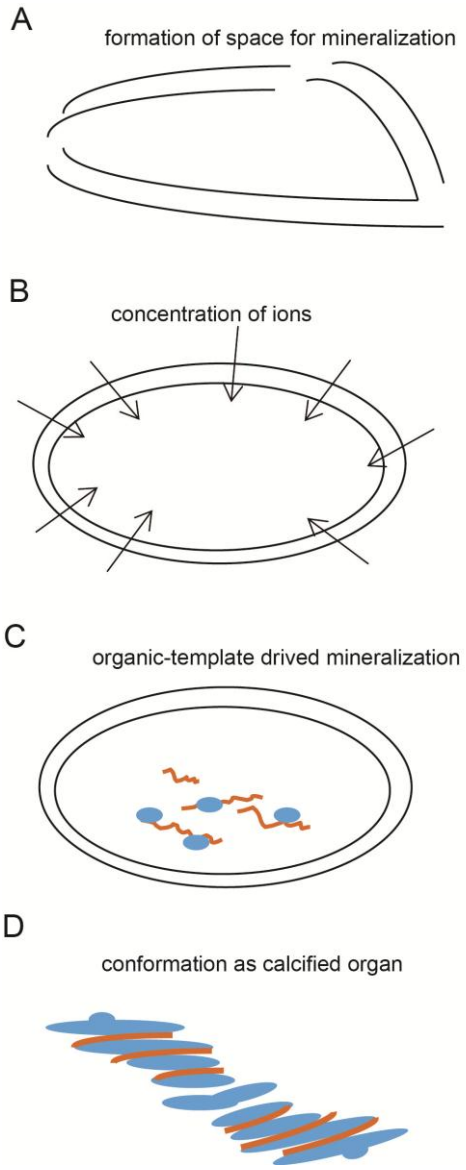

Figure 1. Process of biomineralization. (A) Biomineralization occurs in a closed compartment, intracellular or extracellular, and single cell or multicellular organ. Before crystallization, this special space is configured. (B) Inorganic ions required for mineralization are transferred into the space and concentrated by biological activities such as active transporters. (C) Organic materials (orange) function as a nucleating template and lead to mineral (blue) nucleation and oriented growth. (D) The biomineral is grown there and finally become the functional crystalized tissue within the space or out of the space.

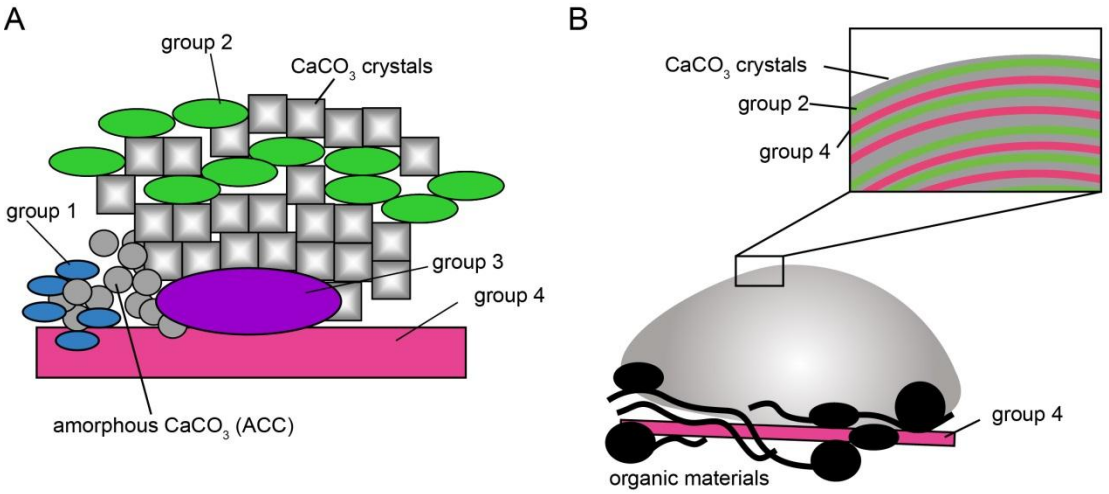

Figure 2. A model for classification of organic matrices in biominerals (example of calcium carbonate) (A) Organic matrices are classified into four groups; group1 – group 4, according to solubility and function. Group1 (blue) stabilizes amorphous state, while group 3 (purple) induce the crystallization and regulate features of crystals by interacting with both amorphous particles and structural matrix (group4, pink). Mineral growth and morphology is regulated by group 2 (green) which partially inhibits the crystallization. Detailed explanation is described in the text and examples are listed in Table 1. (B) Growing minerals are physically supported by complex organic materials (black) including organic matrices in group 4. Biomineral gradually increases its mass by forming organic and crystal layer. Panel (A) is drawn based on the review by Nagasawa (2013) with some modifications.

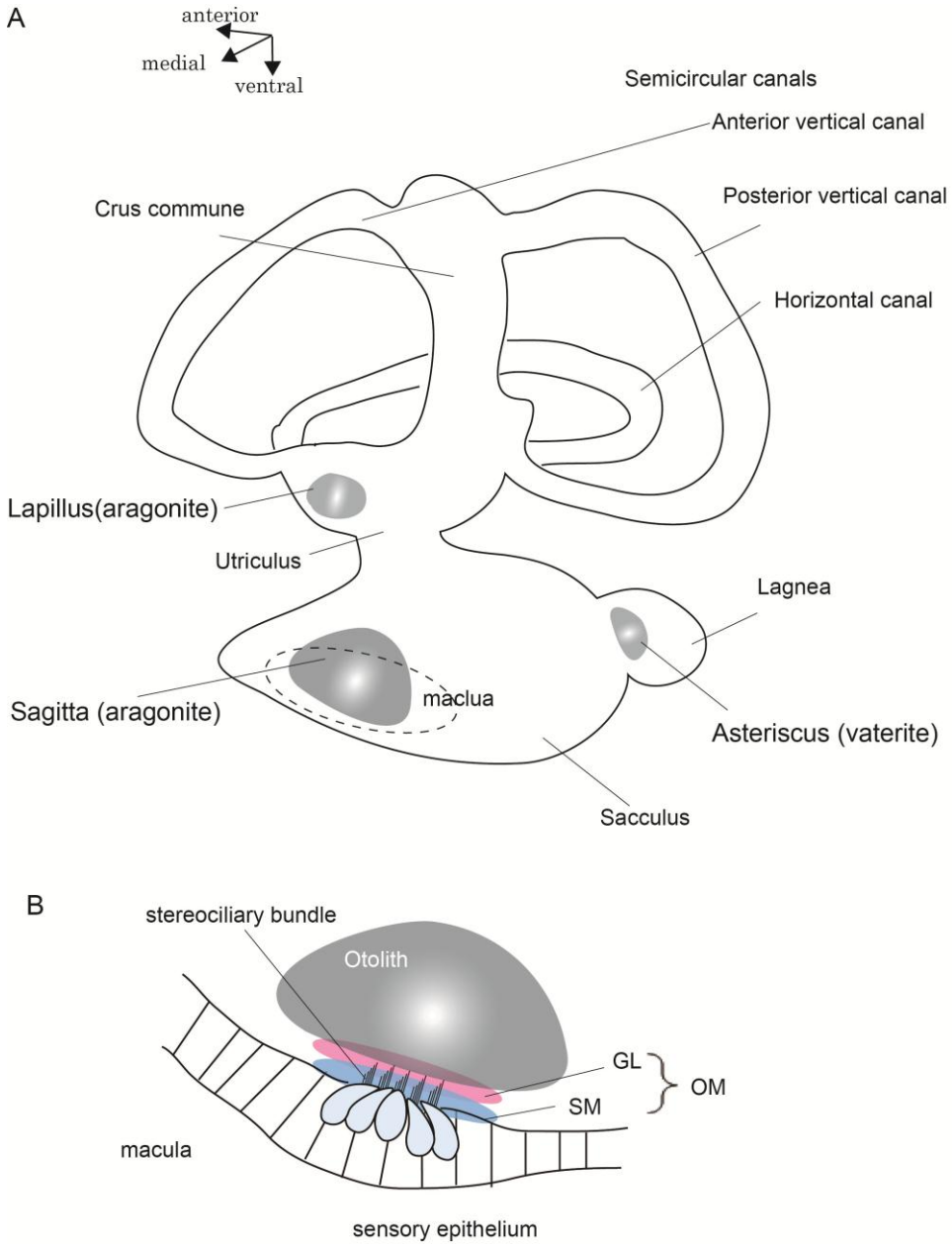

Figure 3. Schematic representation of a fish inner ear with special reference to the location of otoliths. (A) The inner ear of teleost fish consists of three sacs (utriculus, lagena and sacculus) which are connected by semicircular canals. Each sac contains an otolith (lapillus, asteriscus and sagitta, respectively). (B) Otolith sets on a sensory epithelium (macula) covered by the otolithic membrane (OM). OM is composed of abundant extracellular matrices layers, gelatinous layer (GL) and subcuplar meshwork (SM).

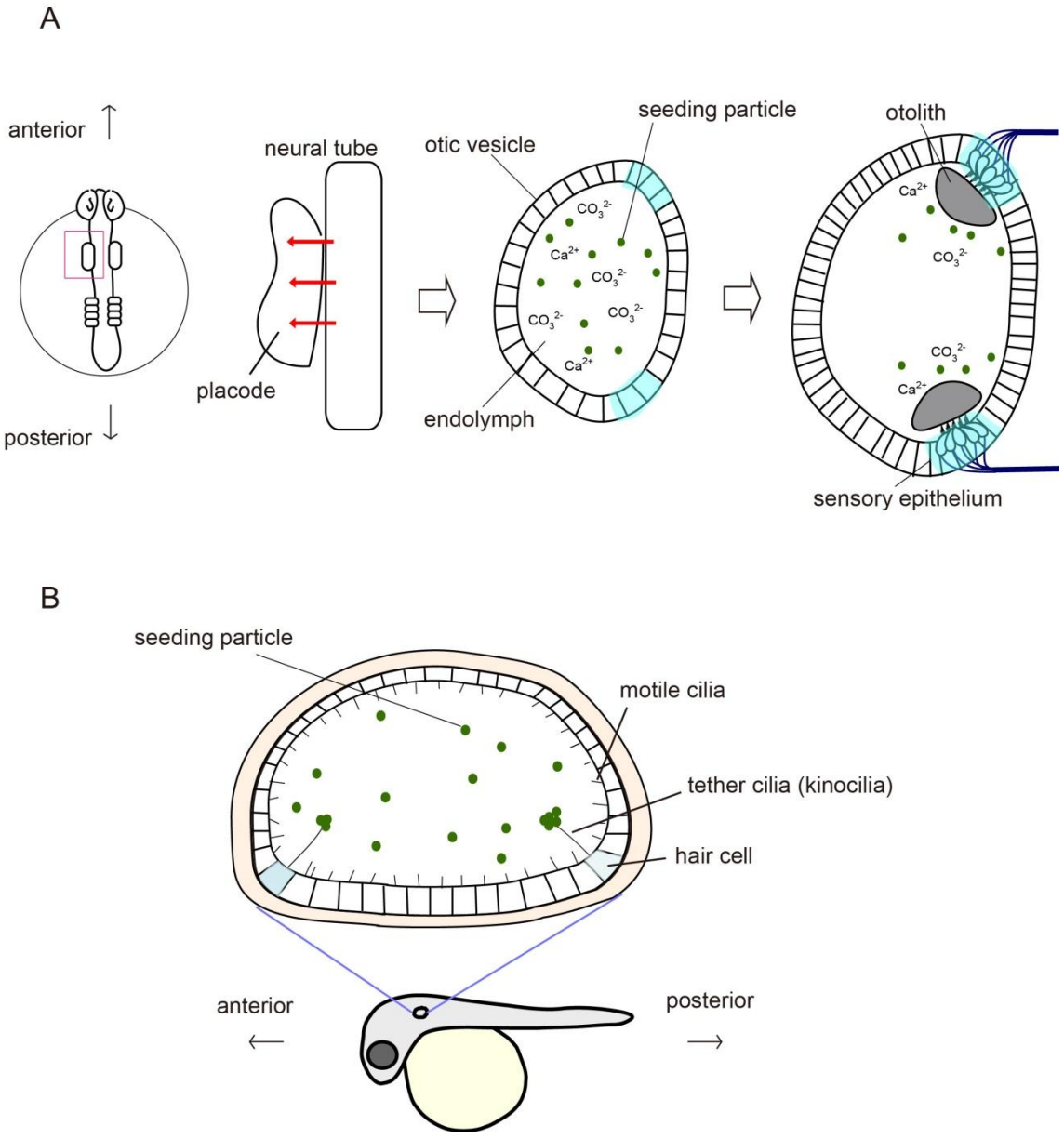

Figure 4. Schematic illustrations of development of zebrafish otic vesicles (OVs). (A) OV, the primordium of inner ear, is formed during somite-formation stage. Otic placode is induced by neural tube, and then it becomes the OV which is composed of single layer epithelium filled with endolymph. Within endolymph, ionic compositions, calcium ion and carbonate ion, are concentrated, and special membranous vesicles, 'seeding particles' are floating. Otoliths are formed at anterior and posterior regions of the OV epithelium, prospective utriculus and sacculus respectively. All drawings are dorsal views. (B) Seeding particles freely floats in endolymph, and are tethered by a special kinocilia (tether cilia). Agitation by motile cilia prevents the seeding particles to aggregate in other places. Lateral view.

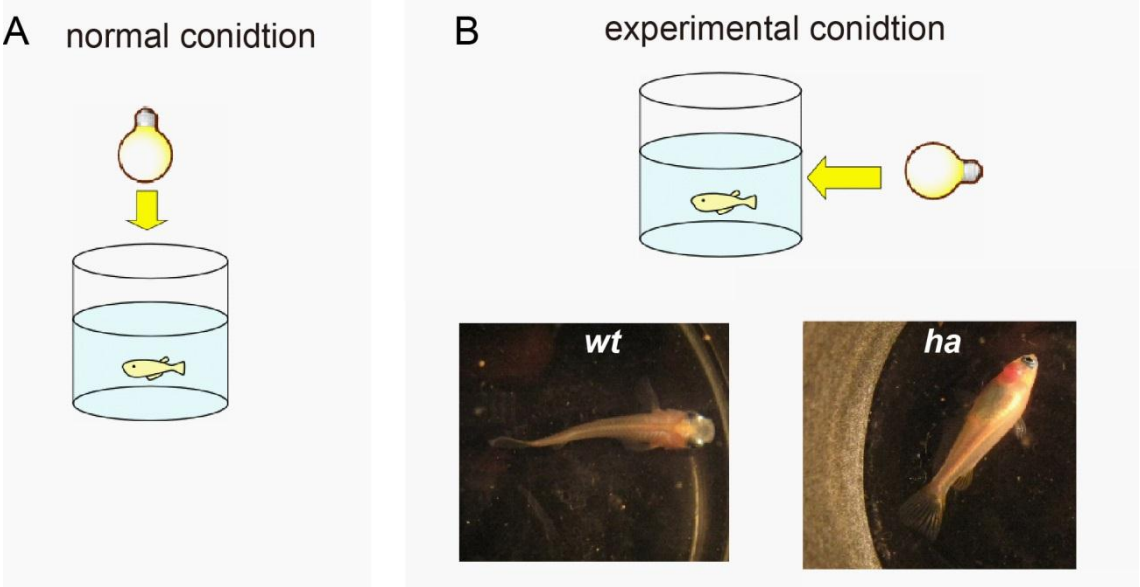

Figure 5. Behavioural abnormality observed in adult *ha* fish. The defect of inner ear, vestibular organ (sacs and otoliths) and semicircular canals, leads to some behavioural abnormalities such as circular swimming. Here, a balance test is descried. (A) *ha* fish are less sensitive to gravity, but their dysequilibrium is compensated by light sensing. They can keep their equilibrium in normal breeding condition. (B) In an experimental condition, in which the aquarium is laterally illuminated, *ha* fish change their body position so that their back is oriented to the direction of illumination. Photographs and schematic diagrams were kindly provided by Dr. Ai Omi.

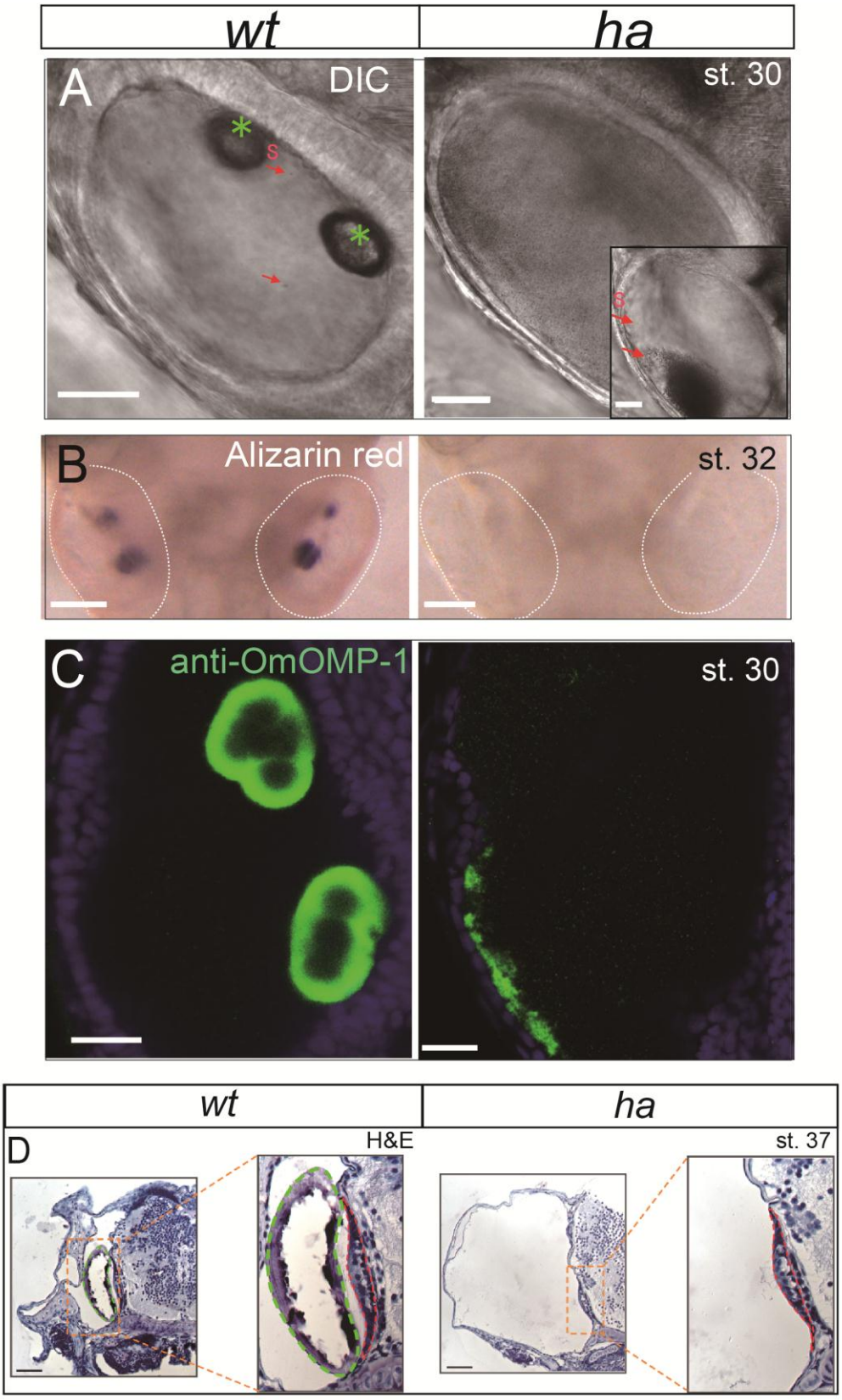

Figure 6. Defects of mineralization in *ha* embryos. (A) DIC images of OVs at st. 30 (dorsal views of the left OV). Grown otoliths are observed in the *wt* OV. The Mutant OV contains

numerous seeding particles that form a paste-like precipitate (*Inset)*. Red arrows: seeding particles; Asterisks: otoliths. Scale bars: 20 μm. (B) Alizarin Red staining for mineralized otolith at st. 32. Crystals are never observed in the mutant OVs (dorsal views of the head; white dotted lines show OV). Scale bars: 100 μm. (C) Immunofluorescence of an otolith matrix protein, OMP-1 (dorsal views of the left OV). Anti-*Oncorhynchus mykiss* OMP-1 (OmOMP-1) serum is used. In the mutant OV, immunoreactive substances cling to the epithelium at st. 30. Scale bars: 20 μm. (D) Saccular ototlih (saggita) is located on the sensory epithelium (macula) in *wt* embryo. *ha* develops normal macula though it has no otolith and OV is enlarged. Hematoxylin and Eosin stain of a cross section of sacculus at st. 37 (Right side shows medial). Green dotted lines: otoliths, red dotted lines: maculae. Scale bar: 40μm. Panel (D) was kindly provided by Dr. Ai Omi.

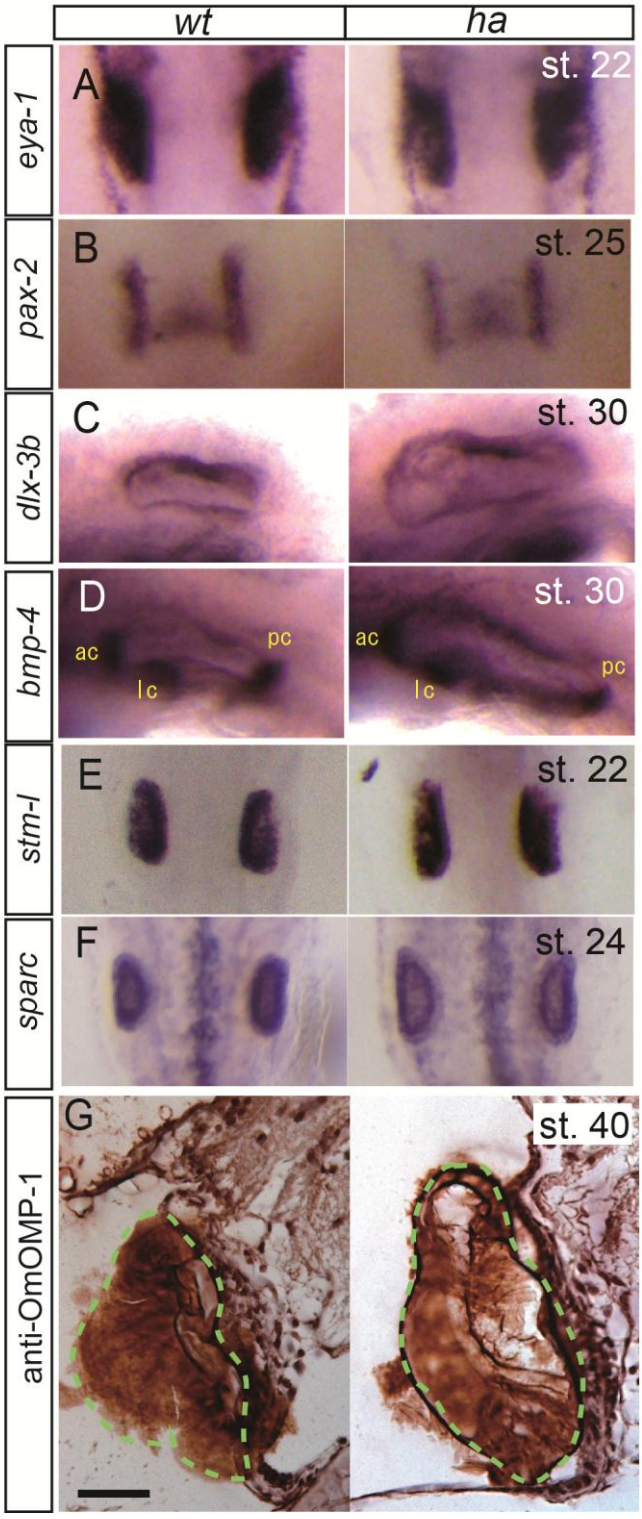

Figure 7. Expression of molecular markers related to inner ear and otolith formation. (A-F) Whole-mount *in situ* hybridization of molecular markers expressed in the OVs. (A and B) Differentiation markers, *eya-1* (across the vesicles) and *pax-2* (medial region) are normally expressed in *ha* embryos. OVs are dorsal views. (C and D) Normal expression patterns of

marker genes at stage st. 30. *dlx-3b* is restricted to the dorsal wall of the OV and *bmp-4* marks the neural cristae regions, showing that regionalization and neural differentiation patterns are not disturbed in *ha* mutant. Mutant OVs are enlarged. ac, anterior cristae; lc, lateral cristae; pc, posterior cristae. OVs are lateral views. Left side shows anterior. (E and F) The transcripts of organic matrix proteins, *starmaker-like* (*stm-1*)(st. 22) and *sparc-1* (st. 24) are comparably detected in the mutant OV. OVs are dorsal views. Mutant OVs are enlarged at st. 24. (G) Cross sections of the maculae of the OV. Immunohistochemistry revealed otolith like stones contains organic matrices (at least OMP-1 protein) in *ha* at hatching stage (st. 40). Green dotted lines: otoliths. Right side shows medial. Scale bar: 30μm

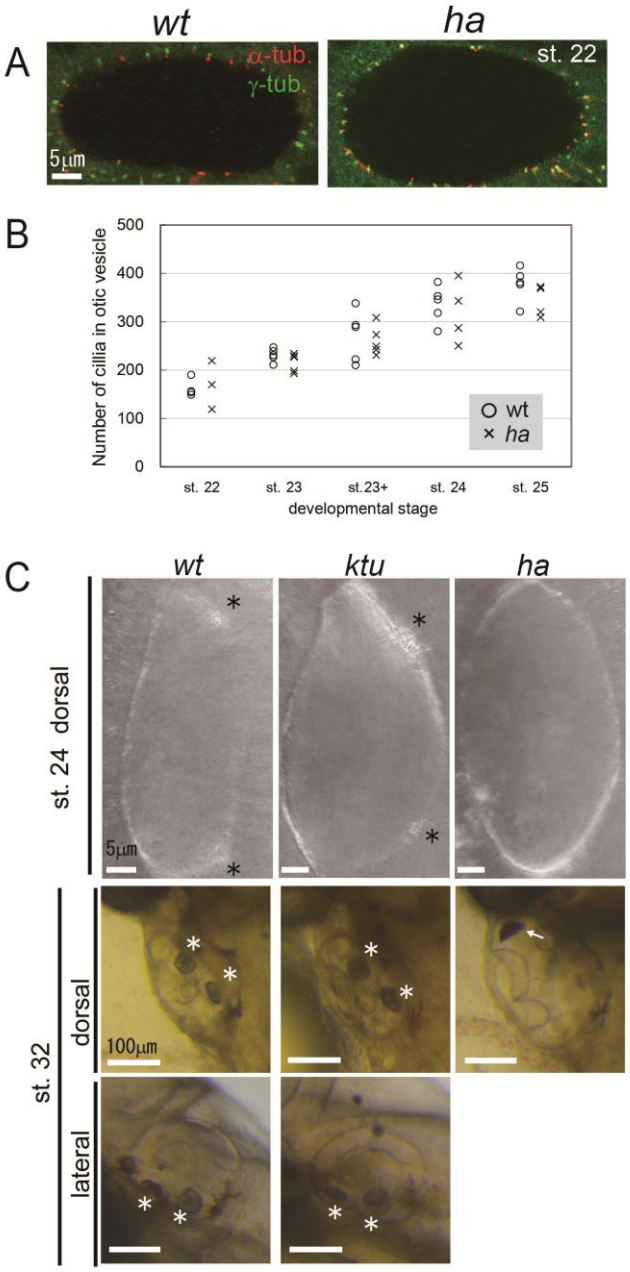

Figure 8. Cilia in medaka OV (A) double colored-Immunofluorescence of acetylated α-tubulin (cilia) and γ-tubulin (root of cilia). Many short cilia (<1μm) are visible in the OV of *ha* as well as *wt*. (B) Scatter plot showing total number of cilia in the OV of *wt* and *ha* at various stages. Total number of cilia in the OV is obtained by counting the signal of α-tubulin and γ-tubulin. In each stage, there is no significant difference in total number of cilia between *wt* and *ha* (>0.05 Student's t-test). (C) Otolith development in the OV of *ktu* mutant. In *ktu*, seeding particles are coalesced at the prospective macula region at st. 24 (*Upper*: dorsal views of left OV), and otoliths appear normal at st. 32 just like *wt* (*Middle*: dorsal views of the left OV and *Lower*: lateral views of the left OV). Asterisks: otoliths, Arrow: paste-like substance

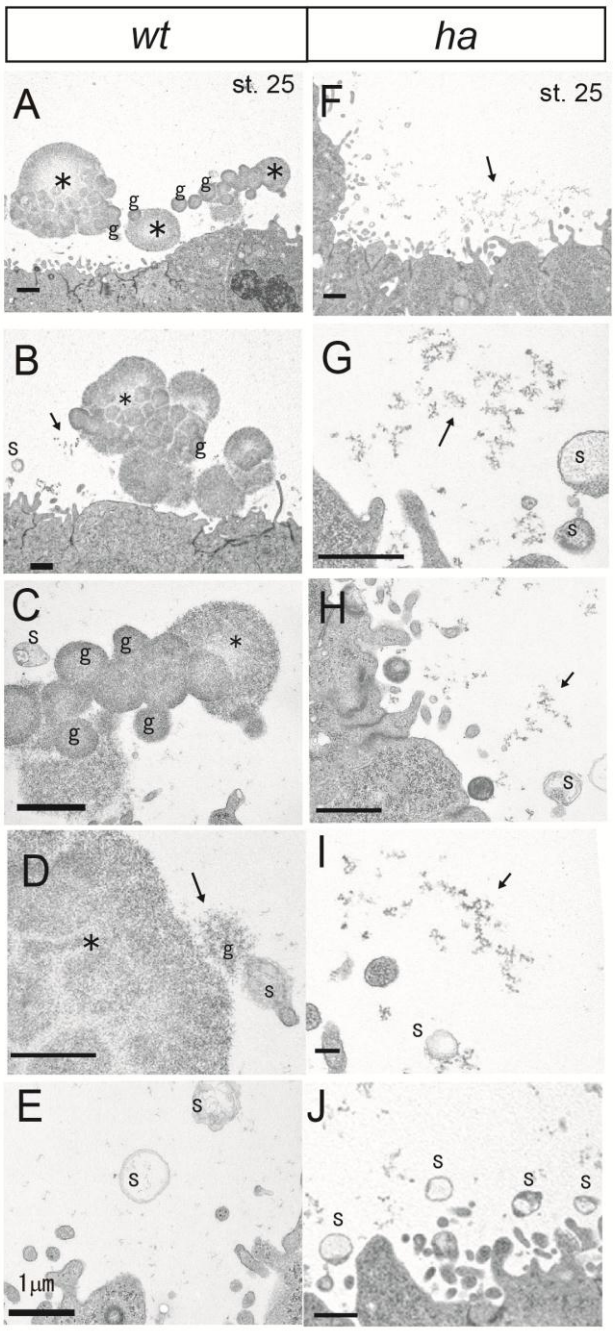

Figure 9. TEM images of the epithelium of the OV at st. 25. (A-E) Representative images at the prospective macula (the posterior end of the OV) of a *wt* specimen. Lateral views. Globules ('g') coalesce to form the otolith (A-C). Very fine particles are supplied by the seeding particles (B and D). Seeding particles are less frequently observed in *wt* OV than in mutant one. (F-J) Representative images at posterior end or mid-position of the OV of a *ha* specimen. Many fine particles accumulated around the epithelial cells (F-I). A large number of seeding particles are observed (J). Asterisks: growing otoliths; Arrows: fine particles; 'g': globule; 's': seeding particle. Scale bars: 1 μm.

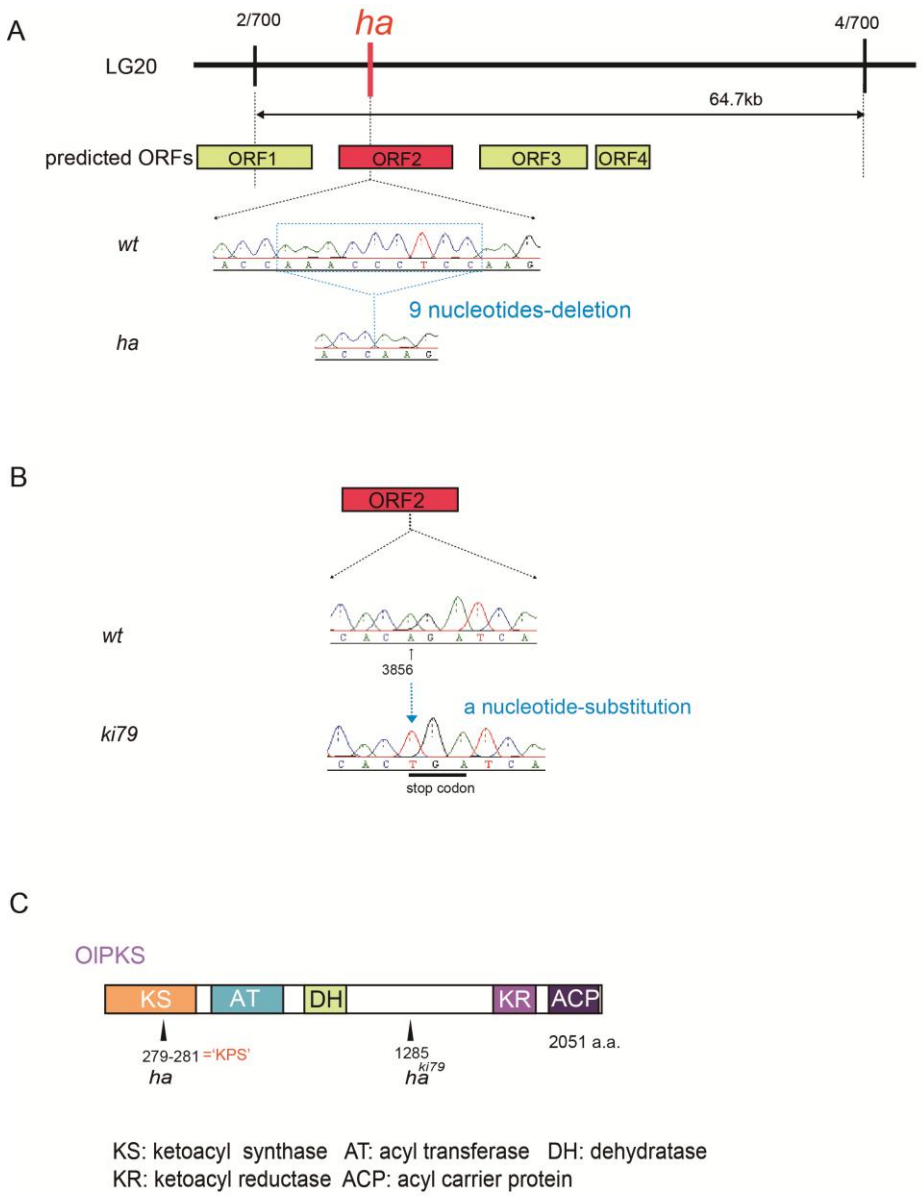

Figure 10. Positional cloning of *ha*. (A) 64.7kb *ha* responsible region (in LG 20) that has been narrowed by recombination analyses is illustrated with predicted ORFs. The number of recombinants at each marker is shown. Sequence comparison between *wt* and *ha* revealed a 9-nucleotide deletion in ORF2. LG: linkage group, ORF: open reading frame. (B) Sequencing of the *ha* gene in another allele, *ki79* fish. *ki79* genome harbours a nonsense mutation at 3856 nt of the ORF 2 locus. (C) Architecture of OlPKS (2051 amino acid-length) predicted by a Pfam search. Each domain is shown by abbreviation. Each arrowhead indicates mutation site of *ha* and *ki79*. The 9-nucleotide deletion in *ha* mutant corresponds to a three amino acids 279-281 (K, P and S).

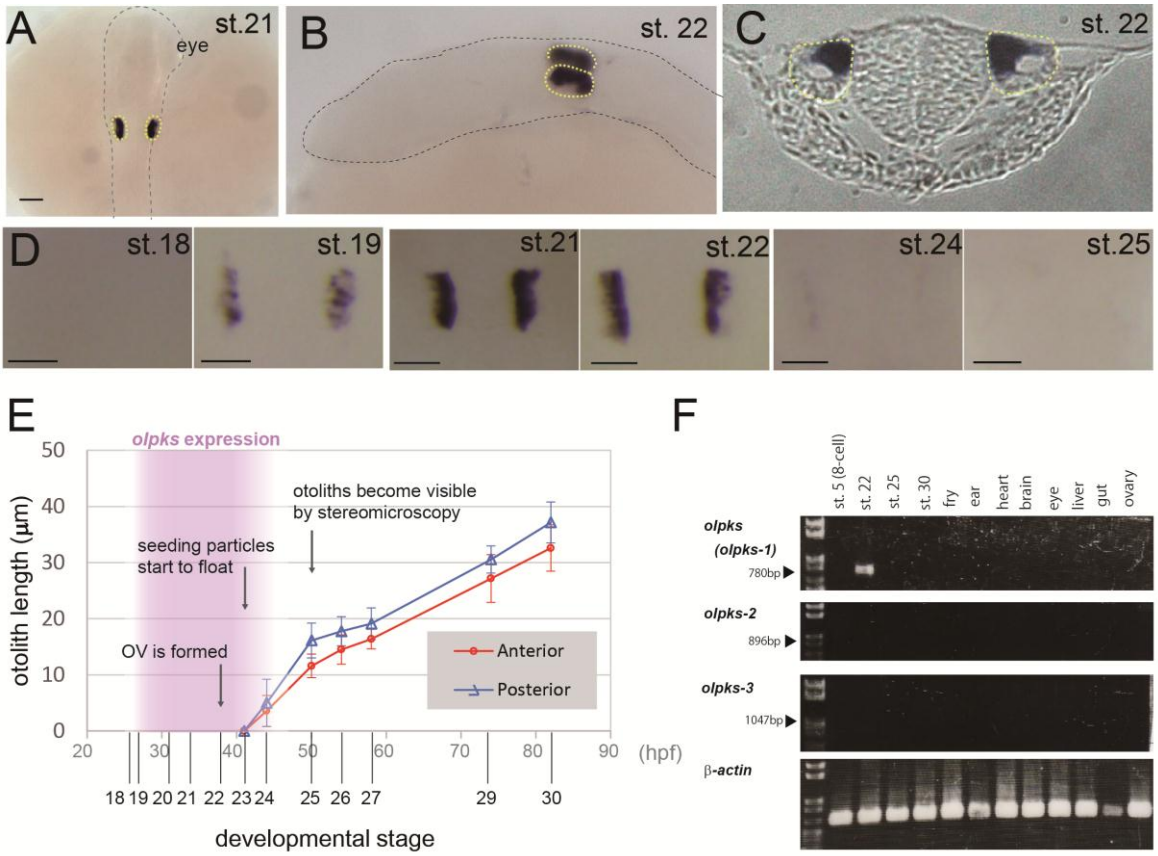

Figure 11. Expression pattern of *olpks*. (A-D) Whole-mount *in situ* hybridization with an antisense RNA probe for *olpks* at otolith forming developmental stages. (A) A representative picture is shown at st. 21 (dorsal view; dotted line indicates embryonic body). (B and C) The dorsally- and medially- restricted pattern is evidenced by lateral view (B) and histology (C) of the OV region. Yellow dashed lines show OVs. (D) *olpks* transcripts detected in various stages are shown at high magnification (dorsal views of left and right OVs). Scale bars: 50 μm. (E) Period of the expression of *olpks* in the context of otolith growth. Purple area shows the period of *olpks* expression. Line graphs show the sizes (longest linear dimensions) of otoliths at some developmental stages. Data are the means and standard deviations of measurements taken of at least 7 specimens each. Some observable changes in the OV during otolith development are described with arrows. Red curcle: anterior otolith; Blue triangle: posterior otolith; hpf: hours post fertilization. (F) Expression profiles of *olpks* and orthologous gene candidates in the embryonic stages or adult tissues. A RT-PCR analysis revealed that *olpks* (*olpks-1*) is expressed but *olpks-2* and *olpks-3* are not expressed and that *olpks* is expressed only around embryonic stage 22. Panel (C) is courtesy of Dr. Ai Omi.

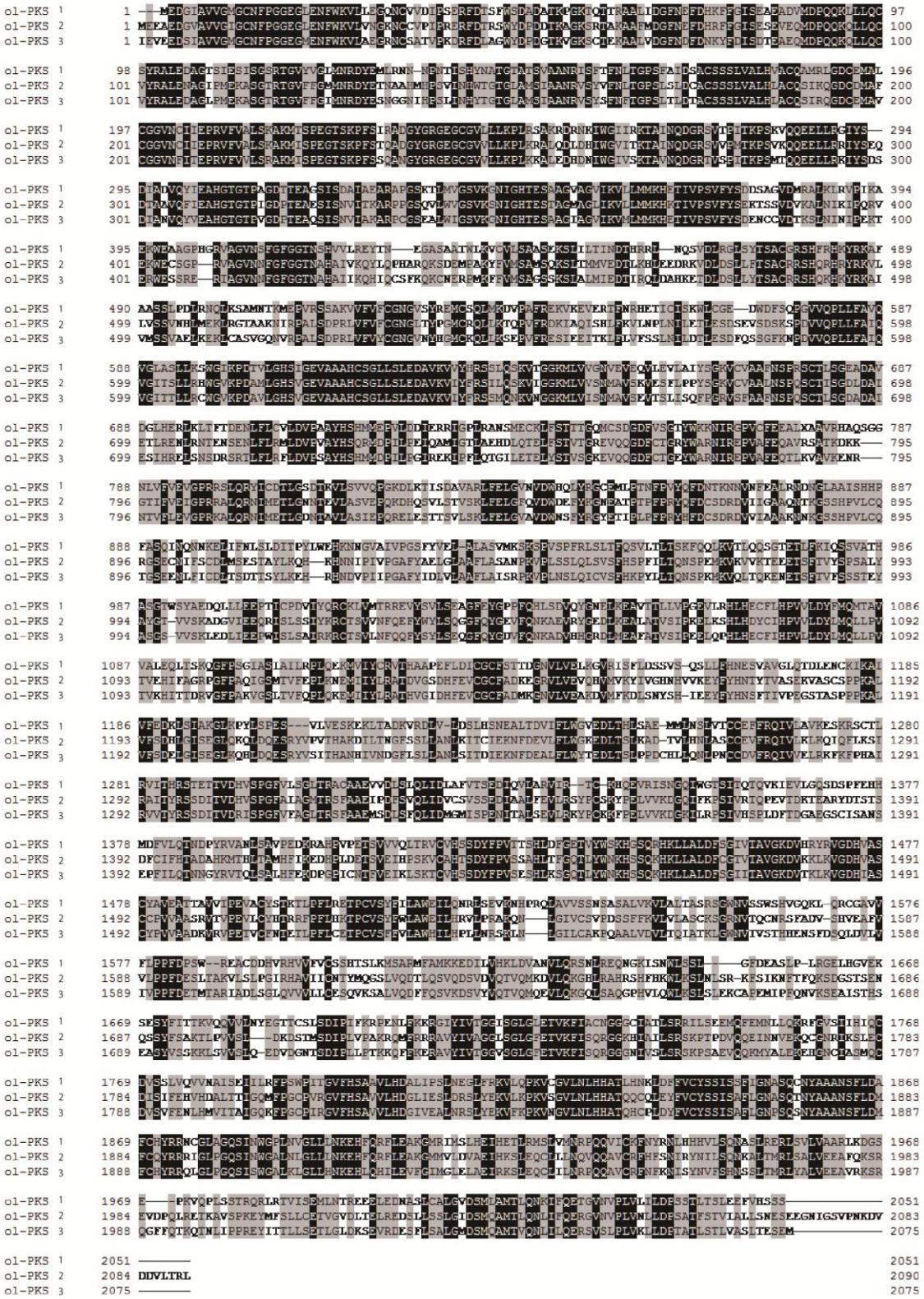

Figure 12. Amino acid sequences of OlPKS and paralogous genes. Predictive paralogous genes, OlPKS-2 and OlPKS-3 are aligned with OlPKS (OlPKS-1). black: identical in all three sequences; glay: identical in two sequences.

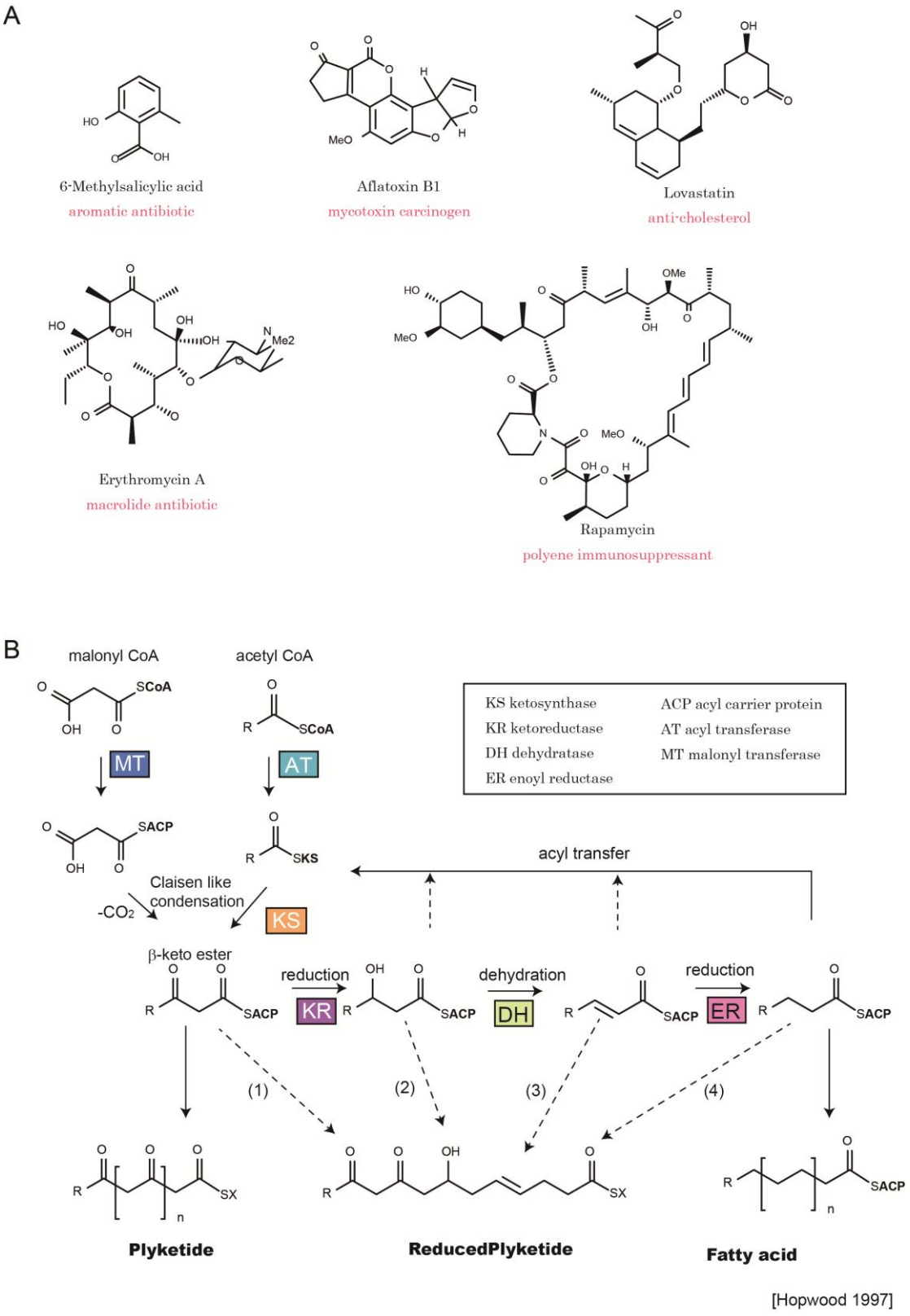

Figure 13. Polyketides and the basic enzymatic pathway catalysed by PKS. (A) Examples of polyketide are shown with reference to the type of polyketide and its biological activity. (B)

Basic pathway of polyketide and fatty acid biosynthesis. (1) - (4) show the alternative versions of the reductive cycles that lead to keto, hydroxy, enoyl, or methylene functionality, respectively, at specific β-carbons during the production of reduced polyketides. The starter unit may be acetyl-CoA or an alternative CoA ester for all classes of synthase, while the chain extender unit is malonyl-CoA (as shown here) for the synthesis of fatty acids and aromatic polyketides, but varies for reduced polyketides (e.g., methylmalonyl CoA, ethylmalonyl CoA). R: $-CH_3$. Panel (B) is drawn based on a review article (Hoopwood, 1997) with some modifications.

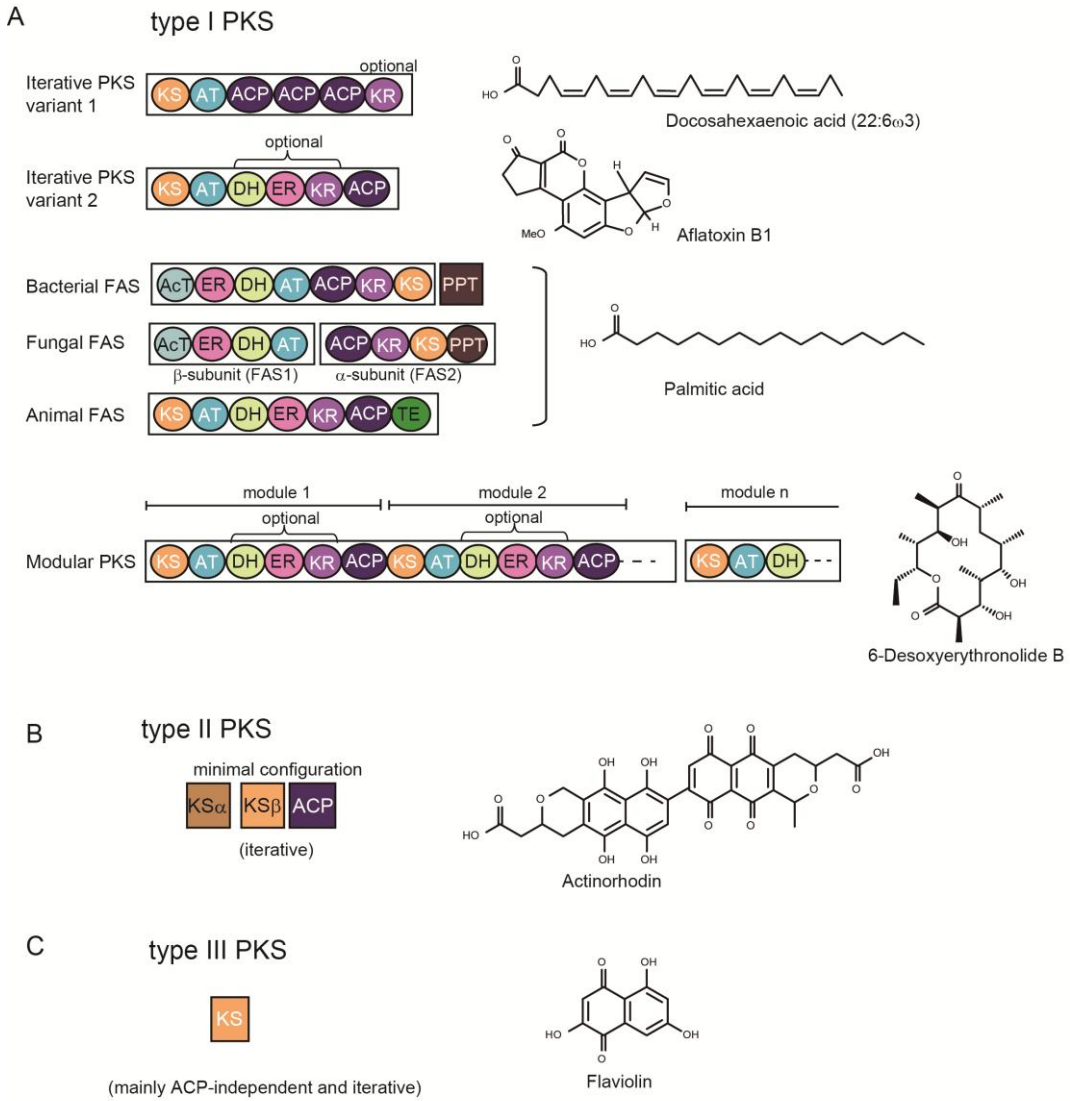

[Jenke-Kodama et al. 2005; Shen 2003]

Figure 14. Types of PKS. (A) Schematic representation of the structure of type I PKSs and FASs. In general, minimal domains are KS, AT and ACP. Optional domains of type I PKS are designated in each case. Patterns of FAS vary depending on organisms. In modular type PKS, only module 1 and 2 are described. Representative product of each type of PKSs is described in right side. (B) In case of type II PKS, each subunit iteratively acts. (C) Type III PKS. Single KS unit iteratively acts. Enzymes additionally required for the synthesis of the respective end products are not shown. Distinct proteins and domains integrated within proteins are shown as squares and circles, respectively. KS, ketosynthase; AT, acyltransferase; DH, dehydratase; ER, enoyl reductase; KR, ketoreductase; ACP, acyl carrier protein; AcT, acetyltransferase; PPT, phosphopantetheinyl transferase. Illustrations are drawn based on the review (Jenke-Kodama et. al., 2005) with some modifications.

A

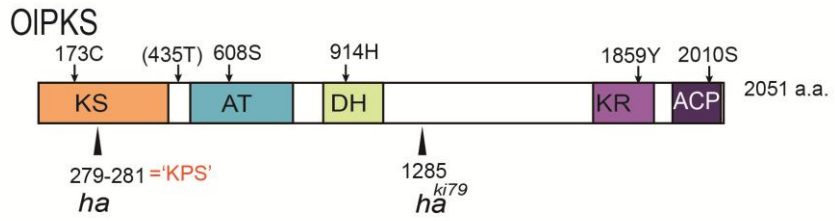

B

Name	Ketoacyl Synthase	Acyl Transferase	Dehydratase	Ketoacyl Reductase	Acyl Carrier Protein
Abbreviation	KS	AT	DH	KR	ACP
Amino acid sequence of OlPKS	*CSSS (173-176) HGTGT (305-109) NIGH (343-346)	GHS*IG (606-610) YHSH (714-717)	*HKNNGVAIVP (914-923) DYEMQ (1078-1082)	TGGISGLG (1714-1721) *YAAA (1859-1862)	*DSML (2009-2012)

asterisks: residues mutated in rescue experiments
underlines: conserved amino acid residues

Figure 15. Domain structure of OlPKS. (A) Architecture of OlPKS protein predicted from the amino acid sequence. Critical residues of each domain used for the mRNA injection experiment are shown by arrows. Mutation site of each mutant is shown by arrowhead. Three amino acids corresponding to 9-bp deletion is 'KPS'. (B) Conserved motifs found in the amino acid sequence of OlPKS. Asterisks show residues mutated in mRNA rescue experiments. Underlines show conserved amino acid residues.

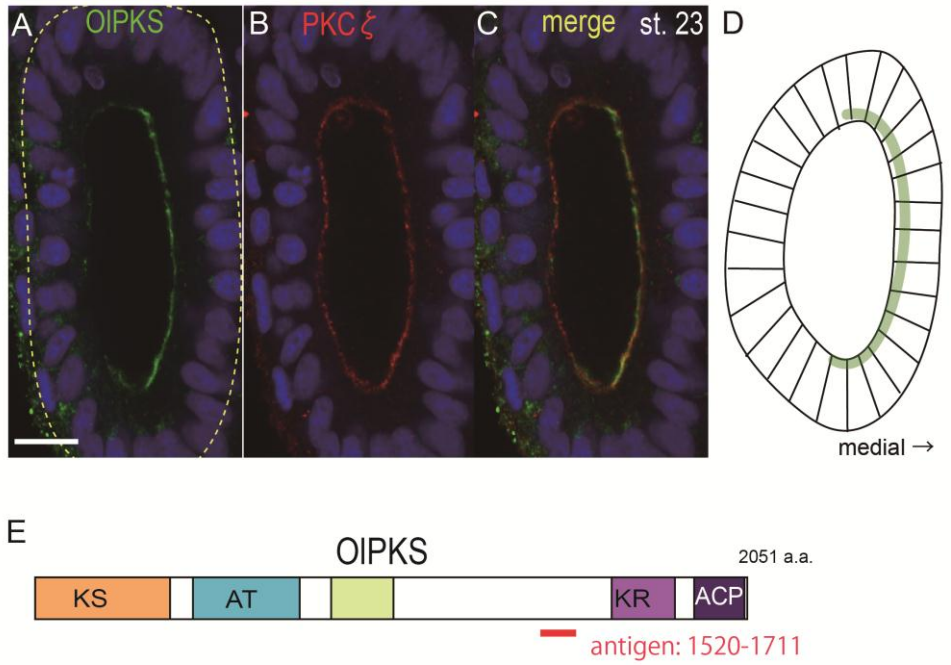

Figure 16. Intracellular localization of OlPKS in the OV epithelium. (A) Anti-OlPKS antibody detects the OlPKS protein at the apical region of the epithelial cells. (B and C) Co-immunostaining with a membrane marker, PKC ζ, shows it localizes near the apical membrane. Blue: nuclei. Dorsal views of the left OV. Yellow dotted line: OV. Scale bar: 10 μm. (D) Schematic illustration of the fluorescent signal of OlPKS in the left OV. (E) The red bar indicates the region used as an antigen for producing anti-serum of OlPKS.

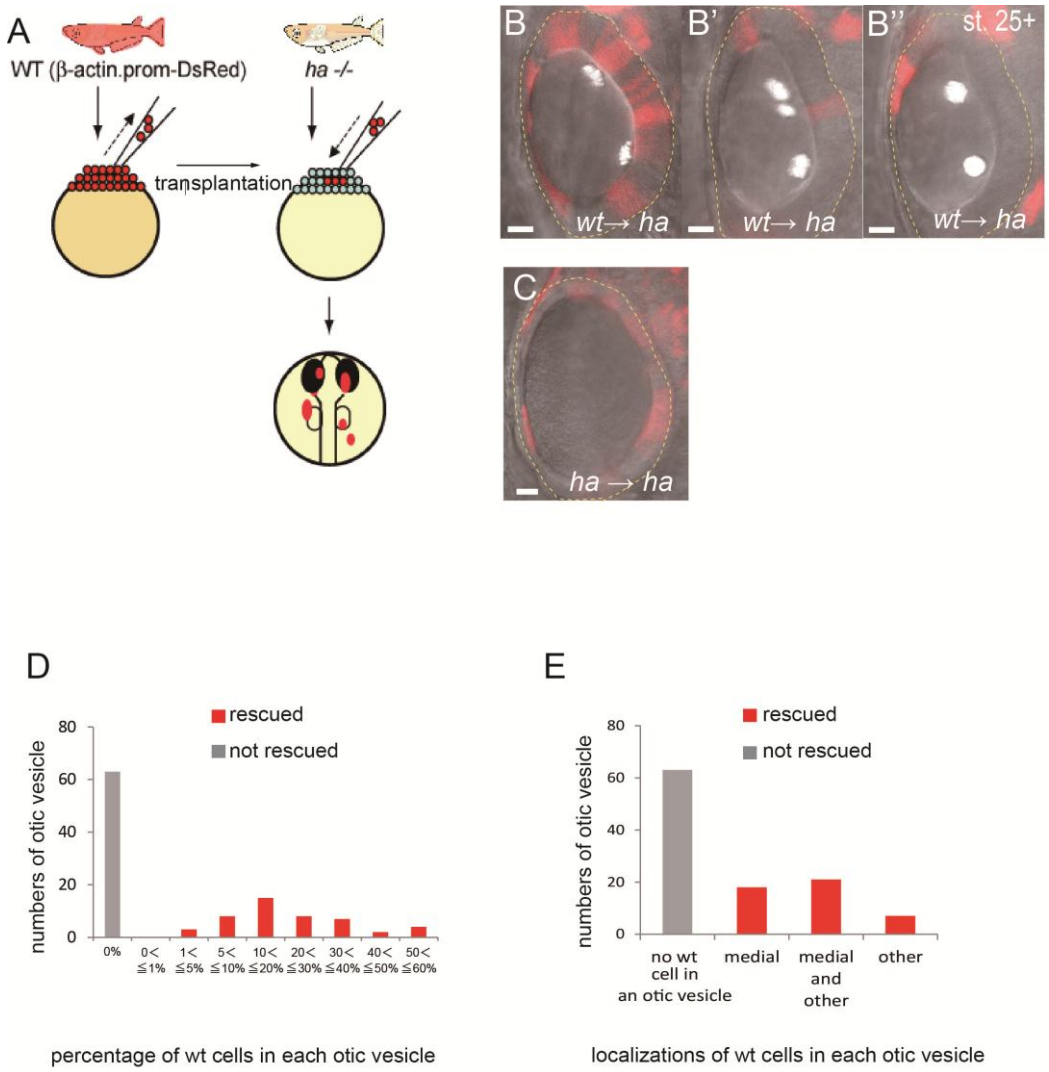

Figure 17. Chimeric experiment. (A) Schematic procedure of the transplantation is depicted. *wt* cells expressing DsRed are implanted to the *ha* embryo. (B-B") Some images of the chimeric OVs in live embryos. [*wt*→*ha*] shows *wt* cells expressing DsRed are transplanted to an *ha* embryo. (C) In negative control experiment, *ha* cells expressing DsRed are implanted to the *ha* embryos shown as [*ha*→*ha*]. Yellow dotted lines: OVs. Scale bars: 10 μm. (D) All 110 OVs of 55 transplanted animals are observed and sorted to 9 categories depending on their percentage of *wt* cells in their OV epithelium (Note a chimeric fish has two OVs). The histogram shows that a very small number of *wt* cells can rescue otolith formation. (E) The same sample set was also analyzed to assess the localization of *wt* cells within the OV. 'medial' means *wt* cells located around medial wall of the OV region where the *olpks* gene is normally expressed in *wt* animals; 'medial and other' includes medial and any other epithelial region; 'other' includes *wt* cells existing anywhere in the epithelium except the medial wall.

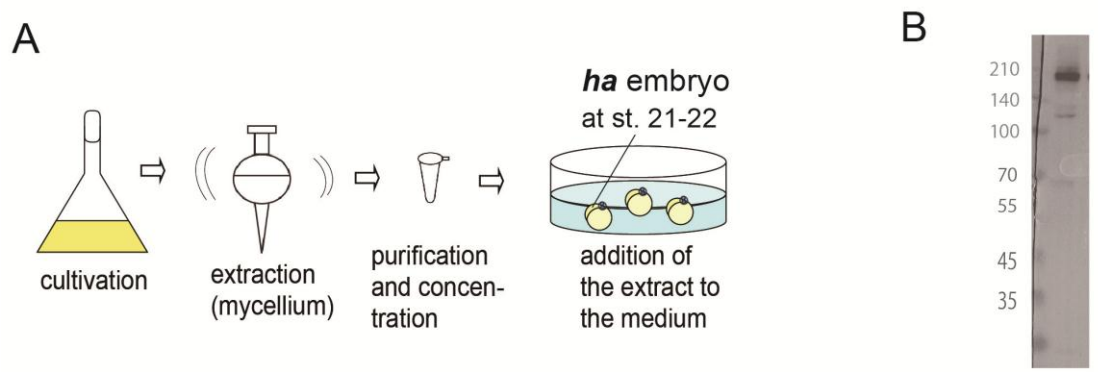

C

extract	4 otoliths (fully rescued)	1-3 otoliths (partially rescued)	no otolith (not rescued)
olpks-transformed	28	4	2
empty vector-transformed	0	0	33

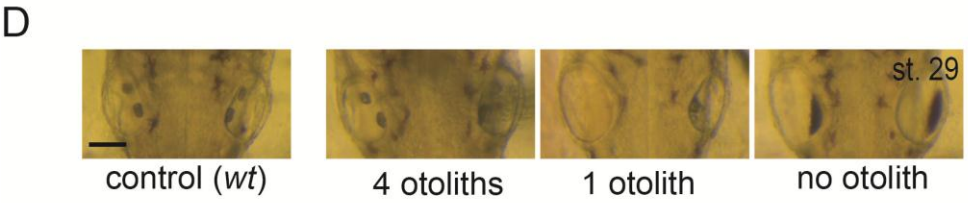

Figure 18. Heterologous expression system. (A) Schematic representation of the rescue experiment by the extract which is generated in the heterologous expression system using *A. oryzae*. (B) Western blot of OlPKS protein produced by *A. oryzae*. To verify expression of OlPKS in heterologous expression experiment, purified protein from a transformant is analyzed by anti-OlPKS antiserum. The OlPKS protein gave a protein band at a position of ca. 210 kDa on SDS-PAGE. Some bands (degradate proteins) were also found in this experiment. (C) Summary of the bioassay in the heterologous expression experiment. Numbers of *ha* embryos treated by the extract of *olpks* transfromant or that of empty vector toransformant are shown. Grades of recovery of the mineralization: 4 otoliths (2 per OV, fully rescued), 1-3 otoliths (at least 1 otolith per embryo, partially rescued) and no otolith (not rescued). (D) Representative pictures of treated embryo in each category is shown with a picture of *wt* embryo. Scale bar: 100 μm.

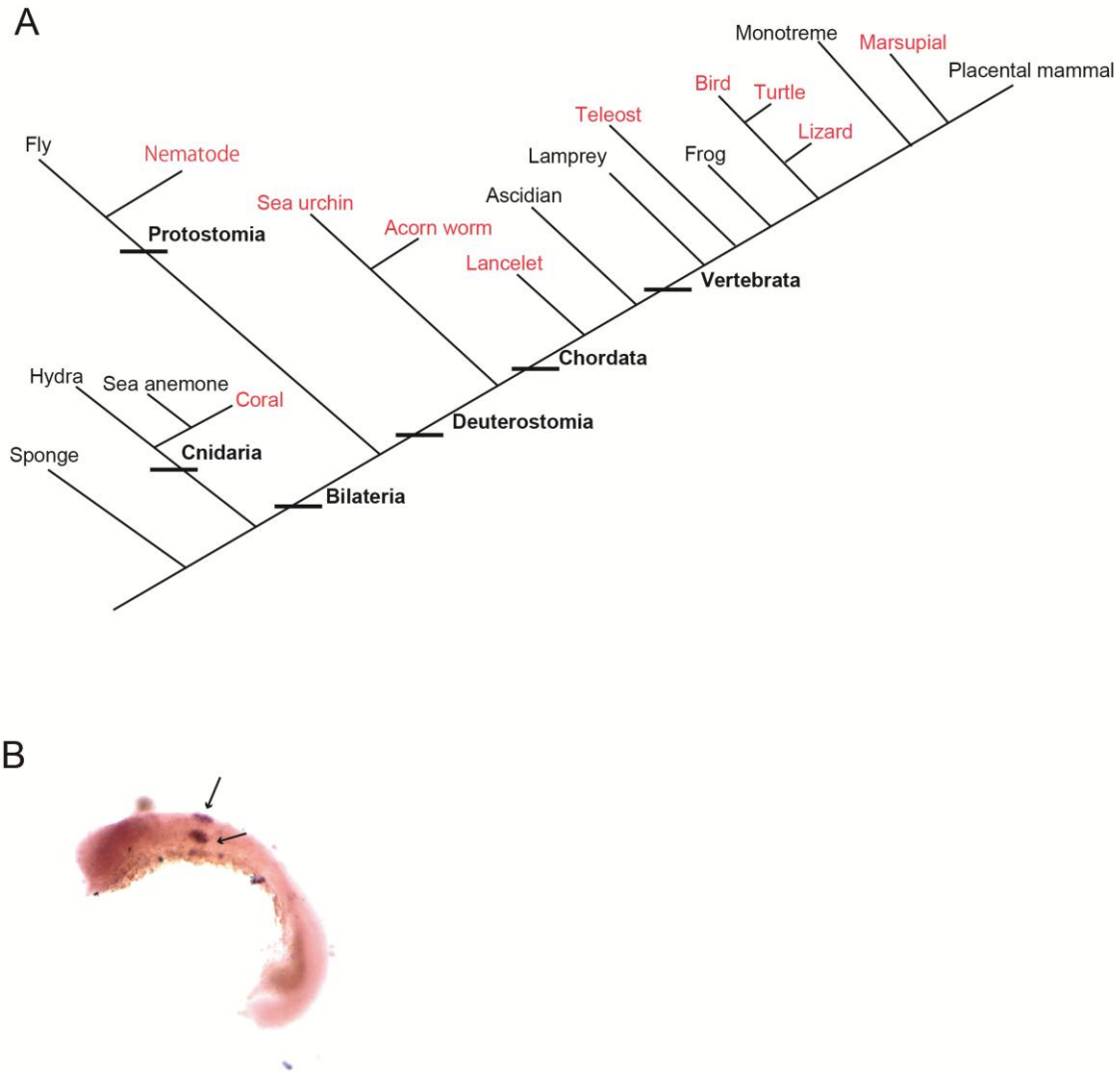

Figure 19. Broad distribution of PKSs in animals. (A) The schematic phylogenetic tree shows presence/absence of type I *pks* gene in animal kingdom. Red font shows the presence of type I *pks* gene(s) in the species. Except for fly, frog and mammal, in the most intensively studied models, *pks* genes could be overlooked due to incomplete genome information. (B) A representative image of whole-mount *in situ* hybridization of zebrafish embryo using probes for zebrafish *olpks*. The transcript of a *olpks* homologue, *drpks(wu:fc01d11)*, is exclusively expressed in zebrafish OV at the 20 somite-stage (19hpf). Arrows: OVs.

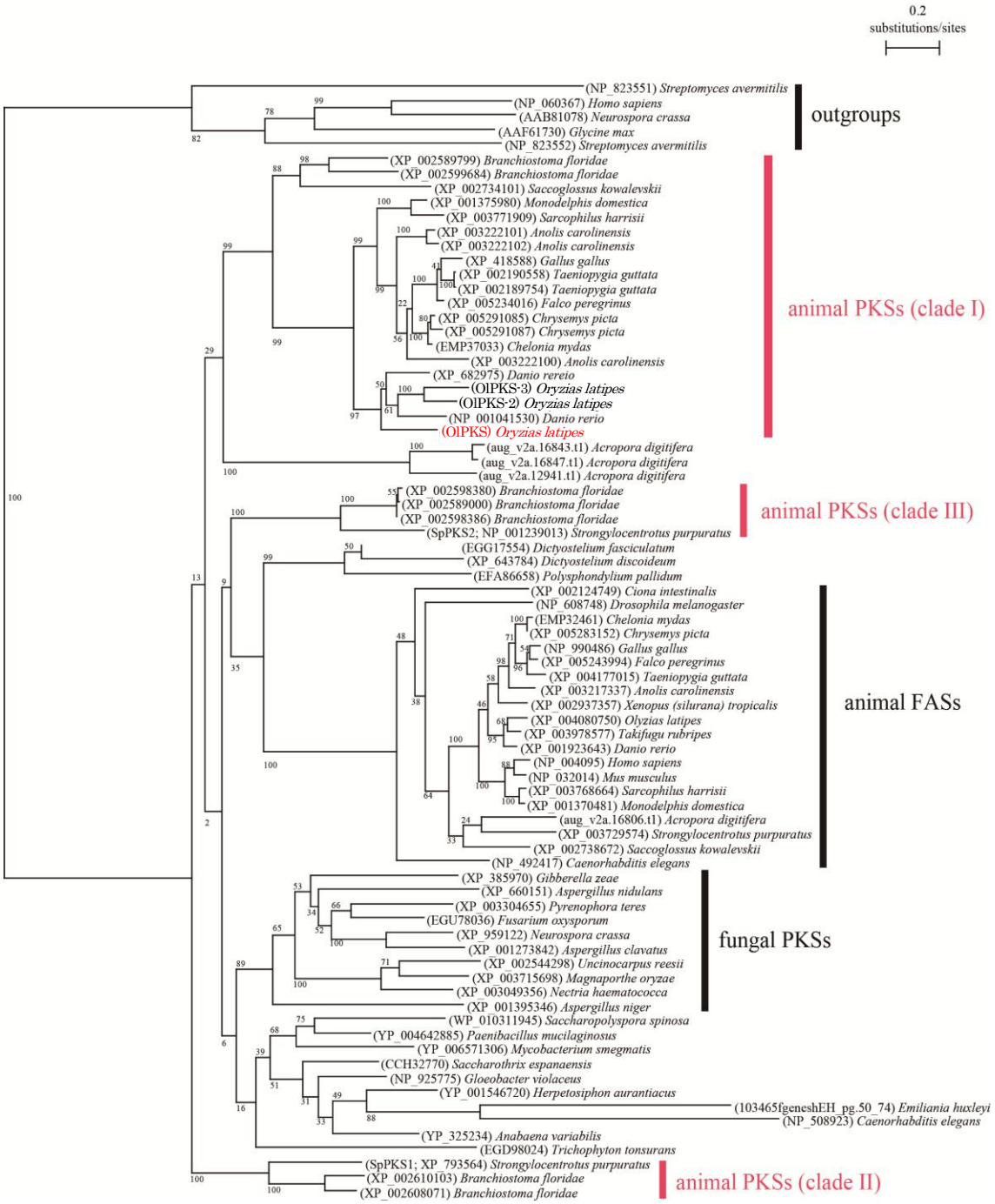

Figure 20. Molecular phylogenetic analysis. A maximum parsimony phylogenetic analysis based on an alignment of amino acid sequences of the KS domain shows relationships among animal type I PKSs and FASs. Animal PKSs containing OlPKS are not divided from other bacterial or fungal PKSs, as indicated by low values of the bootstrap. By contrast, the animal FAS clade is clearly separated from animal PKSs. Protein accession number of

Genbank or other database is shown with species name. Numbers described around branches indicate percentage of the bootstrap value supporting each clade. Branch length indicates number of inferred amino acid changes.

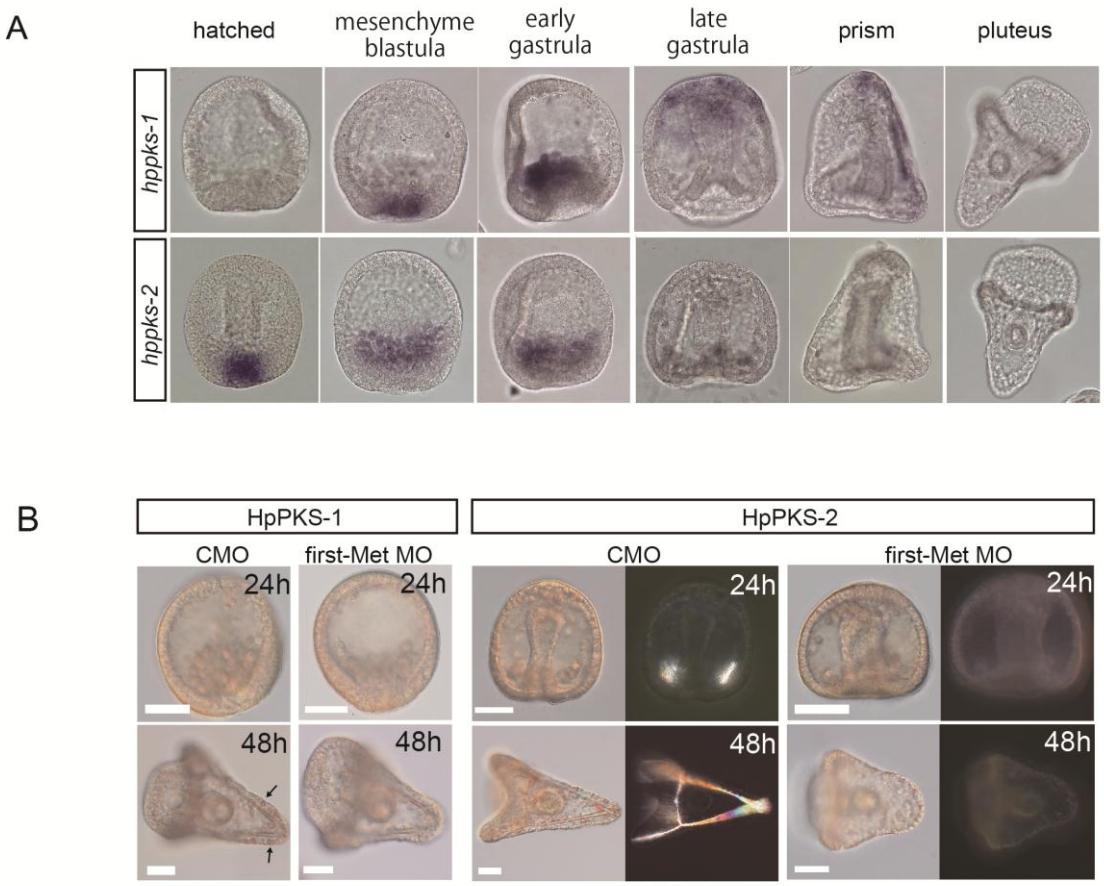

Figure 21. The conserved function found in echinoderm PKS-2. (A) Whole-mount *in situ* hybridization of *H. pulcherrimus* with probes for *hppks-1* (*Upper Panel*) and *hppks-2* (*Lower Panel*). *hppks-1* was first detected at the mesenchyme blastula stage in the precursors of the secondary mesenchyme cells (SMCs) at the vegetal pole, and the expression persisted until the prism stage, in the SMCs and then in the ectoderm. The expression was no longer observed in pluteus larvae. *hppks-2* expression initiates in PMC precursors at the blastula stage and disappear by late gastrula just after spicule formation starting (mid-gastrulation). (B) Representative results of the MO knockdown experiments in *H. pulcherrimus*. Images were taken at two stages (24 h and 48 h). Arrows indicate pigment cells. HpPKS-2 MO-injected or its CMO-injected embryos were also observed by a dark-field microscope for visualizing the spicules. Each MO was injected at a concentration of 200 μM. Scale bars: 50 μm.

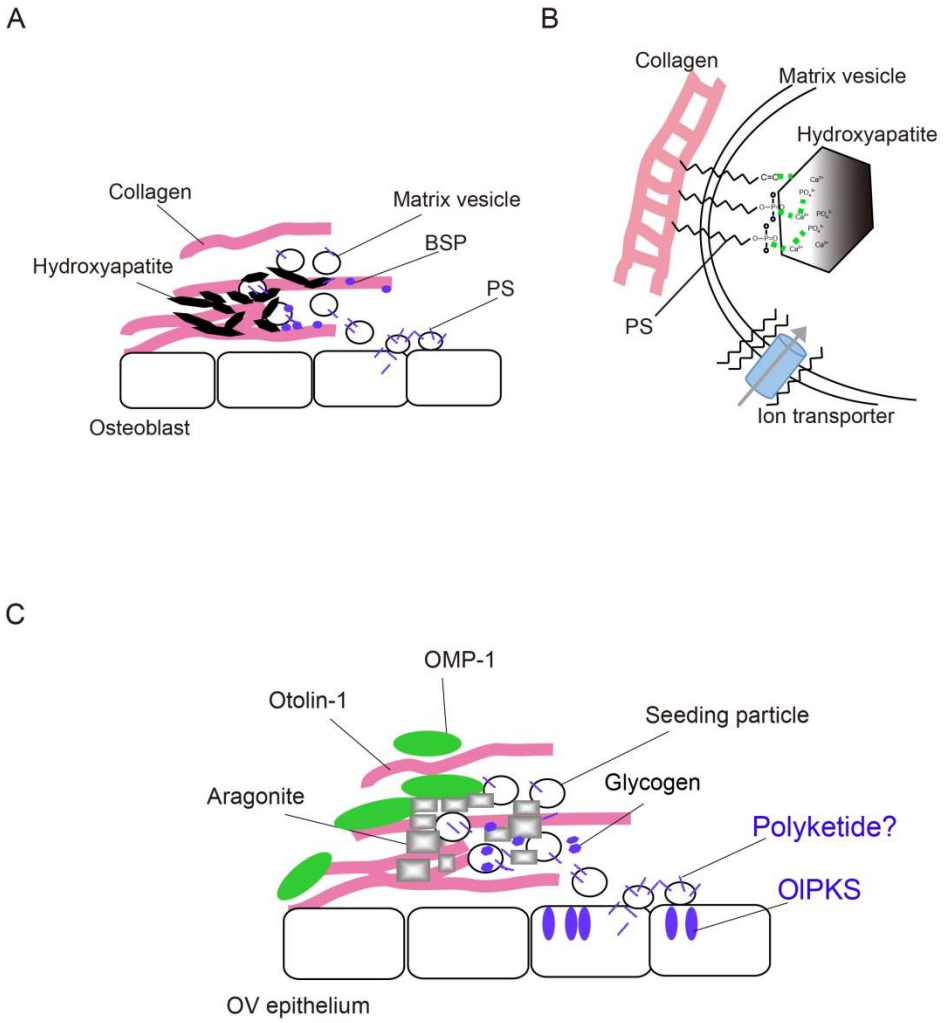

Figure 22. Analogy between bone and otolith. (A) A schematic model of bone nucleation mediated by Matrix vesicle containing PS. PS is conveyed by Matrix vesicle and induces the nucleation of hydroxyapatite together with BSP. PS: phosphatidylserine; BSP: Bone sialoprotein. (B) PS may bridge collagen and nucleating mineral in the membrane of Matrix vesicle. In Matrix vesicle, ions are concentrated by some transporters which is supported by PS. (C) From analogy of PS in bone mineralization, OlPKS product (polyketide?) may be supplied through the seeding particle secretion and it induces the nucleation of aragonite. It possibly bridges otolin-1 (collagen like protein) and the nucleating aragonite, together with some organic material such as glycogen. Panels (A) and (B) are drawn based on previous studies (Wuthier, 1975; Boskey and Posner, 1977; Boyan et al., 1989 Ninomiya and Takahashi, 2008).

A

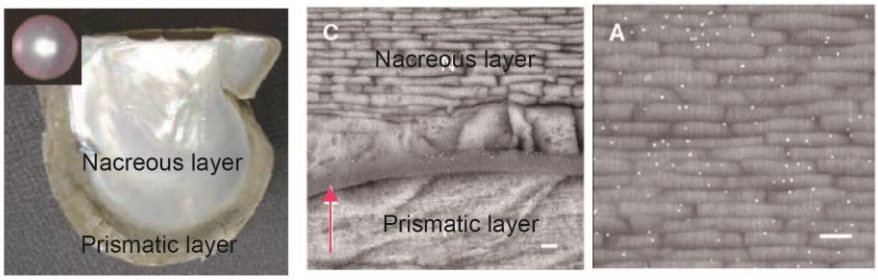

[Suzuki et al. 2009]

B

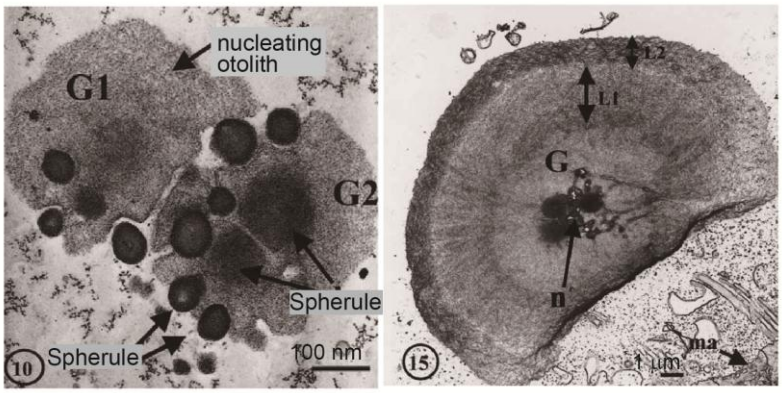

[Pisam et al 2002]

Figure 23. Location of organic matrices nucleation factors. (A) (*Left*) The pearl and shell of *P. fucata.* The shell is consisted by Nacreous layer and prismatic layer. (*Center*) Localization of Pif by means of immunohistochemical-SEM image analysis using gold nanoparticles. Particles are densely located on the organic boundary between the nacreous and prismatic layers (arrow). P, the prismatic layer; N, the nacreous layer. (*Right*) Particles are also distributed through the nacreous layers. (B) TEM images of zebrafish otolith(*Left*) TEM micrographs at 23 hpf shows that some electron-dense spherules are depicted during the process of nucleation. These spherules gradually start to transform into 'globules', described as *G1* and *G2*. (*Right)* TEM section through a 50 hpf ootlith shows the electron dense spherules that make the core (nucleus; n) visible. The fused grobules (*G*) are surrounded by radial layers (L1 and L2). Photographs of (A) and (B) are cited from previous works (Suzuki et al., 2009 and Pisam et al., 2002, respectively) with some modifications.

Tables

Table 1 Organic matrices in biomineralization

group	name(abbreviated)	name(full)	biomineral	function	reference
group1	PEP	phosphoenol-pyruvate	crustacean exoskeleton	ACC-stabilize	1
	3-PG	3-phosphoglycerate	crustacean exoskeleton	ACC-stabilize	
group2	Casp-2	calcification-associated soluble protein-2	crayfish exoskeleton	crystal growth	2
	OMP-1	otolith matrix protein-1	fish otolith	crystal growth	3
	CMAP	coccolith matrix acidic polysaccharide	coccolith	calcification inhibitor	4
	GSP-37	goldfish scale matri protein	fish scale	calcification inihibitor	5
	galaxin	-	coral skeleton	?	6
group3	CAP-1	calcification-associated soluble pepetide-1	crayfish exoskeleton	nucleation	7
	CAP-2	calcification-associated soluble pepetide-2	crayfish exoskeleton	nucleation	8
	Pif80/97	-	nacreus layer of oyster shell	nucleation	9
	Starmaker	-	otoltih	polymorph	10
group4	chitin	-	crustacean exoskeleton	supporting structure	11,12
	cellulose	-	coccolith		
	collagen I	-	bone		
	otolin-1	-	ototlih		

1 (Sato et al., 2011), 2 (Inoue et al., 2007), 3 (Murayama et al., 2000), 4 (Marsh et al., 1992), 5 (Miyabe et al., 2012), 6 (Fukuda et al., 2003), 7(Inoue et al., 2001), 8 (Inoue et al., 2004), 9 (Suzuki et al., 2009), 10 (Sollner et al., 2003), 11 (Nagasawa, 2013), 12 (Murayama et al., 2004)

Table 2 Otolith formation by injections of MO or mRNA

nucleltide	fish	4 otoliths	1-3 otoliths	no otolith	n
olpks first-Met MO	*wt*	0%	0%	100%	39
-	*ha*	0%	0%	100%	31
olpks mRNA		73%	23%	3%	30

4 otoliths: all otoliths are normally formed in one animal (fully rescued)

1-3 otoliths: at least one otolith is formed in one animal (partially rescued)

no otolith: not rescued

n: number of embryos

Table 3 Otolith formation by injections of mutated mRNAs

experiment	mRNA	4 otoliths	1-3 otoliths	no otolith	n
active site mutation	-	0%	0%	100%	14
	olpks mRNA	65%	35%	0%	43
	KS*-mRNA	0%	0%	100%	15
	AT*-mRNA	0%	2%	98%	57
	DH*-mRNA	0%	0%	100%	18
	KR*-mRNA	0%	0%	100%	17
	ACP*-mRNA	0%	0%	100%	27
	Loop*-mRNA	53%	40%	7%	60
FAS-compensation	*fas* mRNA	0%	0%	100%	17
	fas mRNA ⊿TE	0%	0%	100%	50
	fas mRNA KS-swapped	0%	0%	100%	50

4 otoliths: all otoliths are normally formed in one animal (fully rescued)

1-3 otoliths: at least one otolith is formed in one animal (partially rescued)

no otolith: not rescued

n: number of embryos

Asterisks indicate that one amino acid mutation is introduced.

'Loop*-mRNA' indicates that one amino acid mutation is introduced in an interdomain region between KS and AT (see Fig. 15).

Table 4 Type I PKSs found in animal lineage

Type I PKS?	Species name	General name	Gene name	Accession number	Reference genome	Gene ID	Corresponding RNA (Unigene or RNA)?	Domains
	Homo sapiens	human	-	-	Homo sapiens GRCh37.p13	-	-	-
	Bos taurus	cattle	-	-	Bos taurus UMD3.	-	-	-
	Canis (lupus) familiaris	dog	-	-	Canis lupus familiaris CanFam3.1	-	-	-
	Tursiops truncatus	dolphin	-	-	Tursiops truncatus turTru1	-	-	-
	Mus musculus	mouse	-	-	Mus musculus GRCm38.p1	-	-	-
✔	*Monodelphis domestica*	opossum	PREDICTED: phthioceranic/hydroxyphthioceranic acid synthase-like	XP_001375980	MonDom5	LOC100024851	no	KS-AT-DH-KR-ACP
✔	*Sarcophilus harrisii*	tasmanian devil	mycocerosic acid synthase-like [Sarcophilus harrisii (Tasmanian devil)]	XP_003771909	Devil_ref v7.0	LOC100922065	N.A.	KS-AT-DH-KR-ACP
	Ornithorhynchus anatinus	platypus	LOC100091954 fatty acid synthase-like [Ornithorhynchus anatinus (platypus)]	-	Ornithorhynchus_anatinus -5.0.1	LOC100091954 (pseudo gene)	N.A.	N.A. (pseudo gene)
✔	*Gallus gallus*	chicken	PREDICTED: phthioceranic/hydroxyphthioceranic acid synthase-like isoform X2 [Gallus gallus].	XP_418588	Gallus_gallus-4.0	LOC420486	yes(brain; connective, blood)	KS-AT-DH-KR-ACP
✔	*Taeniopygia guttata*	zebra finch	PREDICTED: phthioceranic/hydroxyphthioceranic acid synthase-like [Taeniopygia guttata].	XP_002189754	Taeniopygia_guttata-3.2.4	LOC100231542	no	KS-AT-DH-KR-ACP
			PREDICTED: Taeniopygia guttata phthioceranic/hydroxyphthioceranic acid synthase-like	XP_002190558		LOC100222288	N.A.	KS-AT-DH-KR-ACP
✔	*Falco. peregrinus*	peregrine falcon	PREDICTED: probable polyketide synthase 1-like [Falco peregrinus].	XP_005234016	F_peregrinus_v1.0	LOC101916009	N.A.	KS-AT-DH-KR-ACP
✔	*Anolis carolinensis*	green anole	PREDICTED: phthioceranic/hydroxyphthioceranic acid synthase-like [Anolis carolinensis].	XP_003222100	AnoCar2.0	LOC100564455	no	KS*-AT-DH-KR-ACP
			PREDICTED: phthioceranic/hydroxyphthioceranic acid synthase-like [Anolis carolinensis].	XP_003222101		LOC100564655	no	KS-AT-DH-KR-ACP
			PREDICTED: phthioceranic/hydroxyphthioceranic acid synthase-like [Anolis carolinensis].	XP_003222102		LOC100564856	no	KS-AT-DH-KR-ACP
✔	*Chelonia mydas*	green sea turtle	Phthioceranic/hydroxyphthioceranic acid synthase [Chelonia mydas].	EMP37033	CheMyd_ v1.0	locus_tag: UY3_05838	N.A.	KS-AT-DH-KR-ACP
			Polyketide synthase PksN [Chelonia mydas]	EMP24664		locus_tag: UY3_18267	N.A.	KS*-AT-DH-KR-ACP
✔	*Chrysemys picta*	painted turtle	PREDICTED: uncharacterized protein LOC101936604 [Chrysemys picta bellii]	XP_005291085	Chrysemys_picta_bellii -3.0.1	LOC101936604	N.A.	KS-AT*-DH*-KR-ACP
			PREDICTED: uncharacterized protein LOC101937174 [Chrysemys picta bellii]	XP_005291087		LOC101937174	N.A.	other-KS-AT*-DH*-KR-ACP
✔	*Pelodiscus sinensis*	chinese soft shell turtle	pep:KNOWN_BY_PROJECTION_protein_coding	scaffold no. JH209275.1	PelSin_1.0	ENSPSIG00000004874	no	KS*-AT-DH-KR
	Xenopus (Silurana) tropicalis	tropical clawed toad	-	-	Xenopus (Silurana) tropicalis build 1 genome database (v4.2 assembly)	-	-	-
✔	*Oryzias latipes*	medaka	OlPKS (PREDICTED: phthioceranic/hydroxyphthioceranic acid synthase-like [Oryzias latipes])	XP_004081385	Oryzias latipes ASM31367v1	LOC101169887	no	KS-AT-DH-KR-ACP
			OlPKS-2 (PREDICTED: phthiocerol synthesis polyketide synthase type I PpsD-like [Oryzias latipes])	XP_004081384		LOC101169644	no	KS-AT-DH*-KR-ACP
			OlPKS-3 (PREDICTED: probable polyketide synthase 1-like [Oryzias latipes])	XP_004080917		LOC101170716	no	KS-AT-DH*-KR-ACP
✔	*Danio rerio*	zebrafish	Danio rerio wu:fc01d11 (wu:fc01d11), mRNA.	XP_682975	Danio rerio Zv9	wu:fc01d11	yes(muscle)	KS-AT-DH-KR-ACP
			si:dkey-61p9.11	NP_001041530		LOC100000781	yes(kidney)	KS-AT-DH-KR-ACP
✔	*Takifugu rubripes*	fugu	phthioceranic/hydroxyphthioceranic acid synthase-like	XP_003968201	FUGU5	LOC101079294	no	KS-AT-DH-KR-ACP
			PREDICTED: Takifugu rubripes lovastatin nonaketide synthase-like (LOC101079519), mRNA	XP_003968202		LOC101079519	no	KS-AT-DH-KR-ACP
	Petromyzon marinus	lamprey	-	-	Pmarinus_7.0	-	-	-

Table 4 Type I PKSs found in animal lineage (continued)

Type I PKS?	Species name	General name	Gene name	Accession number	Reference genome	Gene ID	Corresponding RNA (Unigene or RNA)?	Domains
✔	*Branchiostoma floridae*	lancelet	hypothetical protein BRAFLDRAFT_205831, partial [Branchiostoma floridae].	XP_002599684 (= EEN55696)	Branchiostoma floridae v1.0	GeneID:7231796	N.A.	KS-AT-DH-KR
			hypothetical protein BRAFLDRAFT_247081 [Branchiostoma floridae]	*XP_002591573*		Gene ID: 7219804	N.A.	KS-AT-DH*-KR
			hypothetical protein BRAFLDRAFT_90481 [Branchiostoma floridae]	*XP_002589799*		GeneID:7210376	N.A.	KS-AT-DH*-KR-AMP
			hypothetical protein BRAFLDRAFT_96868 [Branchiostoma floridae]	*XP_002598386*		GeneID:7254845	N.A.	KS-AT-DH-KR*-TE-C-AMP
			hypothetical protein BRAFLDRAFT_96863 [Branchiostoma floridae]	*XP_002598380*		GeneID:7248951	N.A.	KS-AT-DH-KR*-ACP-TE-C-AMP
			hypothetical protein BRAFLDRAFT_87472 [Branchiostoma floridae]	*XP_002589000*		GeneID:7246004	N.A.	KS-AT-DH-KR*-ACP-C-AMP
			hypothetical protein BRAFLDRAFT_125690 [Branchiostoma floridae]	*XP_002610053*		GeneID:7207083	N.A.	KS*-AT-DH-KR*-ACP*-TE-C
			hypothetical protein BRAFLDRAFT_91451 [Branchiostoma floridae]	*XP_002608071*		GeneID:7214024	N.A.	KS-AT-DH-MT-ADH-KR-ACP-α
			hypothetical protein BRAFLDRAFT_87410 [Branchiostoma floridae]	*XP_002605916*		GeneID:7243248	N.A.	KS-AT-DH-MT-ADH-KR-ACP
			hypothetical protein BRAFLDRAFT_89867 [Branchiostoma floridae]	*XP_002610100*		GeneID:7206066	N.A.	KS-AT-DH-MT-ADH-KR-ACP
			hypothetical protein BRAFLDRAFT_87413 [Branchiostoma floridae]	*XP_002605913*		GeneID:7246000	N.A.	KS-AT-DH-MT-ADH-KR-ACP
			hypothetical protein BRAFLDRAFT_125650 [Branchiostoma floridae]	*XP_002610103*		GeneID:7207596	N.A.	AMP-KS-AT-DH-MT-ADH-KR-ACP
			hypothetical protein BRAFLDRAFT_71890 [Branchiostoma floridae]	*XP_002613500*		GeneID:7224978	N.A.	KS*-AT-DH
✔	*Saccoglossus kowalevskii*	acorn worm	PREDICTED: fatty acid synthase-like	XP_002734101	Skow_1.1	LOC100373061	N.A.	KS*-AT-DH-KR-ACP-C-AMP
	Ciona intestinalis	ascidian	-	-	Ciona intestinalis KH	-	-	-
✔	*Strongylocentrotus purpuratus*	purple sea urchin	LOC588806 probable polyketide synthase 1-like [Strongylocentrotus purpuratus (purple sea urchin)]	*XP_793564.2*	Spur_3.1	LOC588806	yes	KS-AT*-DH*-MT-ADH-KR*-ACP
			LOC592147 polyketide synthase 2	*NP_001239013.1*		LOC592147	yes	KS-AT-DH*-KR-ACP-TE
✔	*Acropora digitifera*	coral	*aug_v2a.12941.t1 aug_v2a.12941 scaf5202:2805-26950(-)*	aug_v2a.12941	Adig_1.0	*aug_v2a.12941*	N.A.	other-KS-AT-DH-KR-ACP*-TE
			aug_v2a.16843.t1 aug_v2a.16843 scaf8086:11276-29700(-)	aug_v2a.16843		aug_v2a.16843	N.A.	other-KS-AT-DH-KR-TE
			aug_v2a.16847.t1 aug_v2a.16847 scaf8086:95926-115499(-)	aug_v2a.16847		aug_v2a.16847	N.A.	other-KS-AT-DH-KR-TE
	Nematostella vectensis	sea anemone	-	-	Nematostella vectensis v1.0	-	-	-
	Hydra magnipapillata	hydra	-	-	Hydra magnipapillata Hydra_RP_1.0	-	-	-
	Amphimedon queenslandica	sponges	-	-	Amphimedon queenslandica v1.0	-	-	-
✔	*Caenorhabditis elegans*	nematode	Protein C41A3.1 [Caenorhabditis elegans]	NP_508923	Caenorhabditis elegans WBcel235	C41A3.1	yes	KS-KS-DH-ACP-KS-ACP-ACP-KR-ACP-AT-DH-KS-KR-KS-AT-ADH-ACP-C-AMP-ACP-TE
	Drosophila melanogaster	fruit fly	-	-	Drosophila melanogaster Release 5	-	-	-

Astarisks show a domain lacking a residue of the active site that is contained in OlPK.

Sequence sources are mainly NCBI protein database, except dolphin, chinese soft shell turtle, lamprey, coral and sea anemone.

KS: ketoacyl synthase, AT: acyl transferase, DH: dehydratase, KR: ketoreductase, ACP: acyl carrier protein domain, TE: thioesterase, AMP: AMP-binding site, MT: methyltransferase, ADH: alcohol dehydrogenase, C: condensation domain

Materials and methods

Fish strains and mapping

The medaka (*Oryzias latipes*) d-rR strain was used as a *wt*. *ha* was isolated as a spontaneous mutant by Hideo Tomita (Tomita, 1990). *kintoun* (*ktu*) was isolated as a LR axis-mutant from ENU-mediated mutant screening (Omran et al., 2008). *ki79* was isolated from a ENU-mediated mutant screening at the Tokyo Institute of Technology, Japan. Mapping of the *ha* locus was carried out as previously described (Kimura et al., 2004; Takeda and Shimada, 2010).

Observation of seeding particles

Embryos were dechorionized and mounted in 2% low-melting point agarose in a glass-bottom petri dish. Seeding particles were observed at the rate of 1 frame per second using a confocal microscopy (Zeiss, LSM 710).

Otolith staining

Alizarin Red staining for visualizing mineralized otoliths was essentially done as described (Ohtsuka et al., 2004). Embryos were fixed with 4% PFA / 2xPBS (Phosphate buffered saline) containing 1% sodium hydroxide for 3 hours at room temperature. The samples were then washed with PBS several times, and stained with 2% Alizarin Red S/1 % sodium

hydroxide solution overnight at room temperature. After quickly washing with 0.5% KOH, samples were mounted in 80% glycerol.

Immunofluorescence

Immunofluorescence for OMP-1 was performed as previously described Murayama *et al.* (Murayama et al., 2005), whereas staining for acetylated α-tubulin, γ-tubulin, OlPKS and PKCζ were done as previously described by Kamura *et al.*(Kamura et al., 2011). Polyclonal rabbit OlPKS [amino acids 1520-1711] antibodies were raised by immunization of rabbits with bacterially expressed His-tagged truncated proteins.

For OMP-1 staining, embryos were fixed with 4% paraformaldehyde/PBS (phosphate buffered saline) overnight at 4°C. After washing with PBST (0.1% TritonX-100 in PBS), the samples were dehydrated with methanol and stored at -20°C. The samples were rehydrated with PBST, then treated with the blocking solution (5% sheep serum, 0.2% BSA in PBST) for 2 hours at room temperature. Primary and secondary antibodies were diluted in blocking solution. As a primary antibody, anti-rainbow trout (*Oncorhynchus mykiss*) OMP-1 serum was used at a 1:500 dilution (Murayama et al., 2005). The embryos were incubated with the serum overnight at 4°C. After washing with PBST for at least 2 hours, the embryos were blocked again then incubated overnight with Alexa 488

(Molecular Probes) conjugated secondary antibodies at a 1:400 dilution.

For acetylated α-tubulin, γ-tubulin, OlPKS and PKCζ, embryos were fixed with methanol/DMSO mixture (methanol:DMSO = 4:1) for 15 minutes at 4°C, blocked in 2% BSA/PBSDT (10% DMSO/0.2% Triton X-100/PBS) and incubated with primary antibodies in 2% BSA/PBSDT overnight at 4°C: α-tubulin (Sigma-Aldrich, T6793) at a 1:200, γ-tubulin (Sigma-Aldrich, T3220) at a 1:200, anti-OlPKS serum at a 1:50 dilution; PKC ζ (Santa Cruz, sc216-G) at a 1:50 dilution. For OlPKS and PKCζ, after washing with PBSDT, embryos were incubated with Alexa 488 or Alexa 555 or Cy5 (Chemicon) conjugated secondary antibodies at a 1:400 dilution. Washed embryos were transferred in 50% glycerol/PBS and photographed using a LSM710 confocal fluorescence microscope (Zeiss).

Immunohistochemistry.

For histological analysis, larvae were fixed 4% PFA/PBST for 3 hours and incubated in 10% EDTA/PBS for 2 days to decalcify. Specimens were embedded in Technovit 8100 (Heraeus Kulzer) and cut into 6 μm thick sections. Sections were treated with 1.5% H_2O_2 to block endogenous peroxidase. After sections were washed in PBST, they were blocked with 2% goat serum diluted in PBS. Primary antibody (OmOMP-1) was diluted in PBS (1:8000)

and incubated for overnight at 4°C. After incubation, sections were washed and incubated with secondary antibody (anti-rabbit IgG-Biotin; Sigma-Aldrich, B7389) overnight at 4°C. After washing, sections were incubated with an ABC Kit solution (Vector, #PK6101) for 15 minutes at room temperature. Finally, they were rinsed in PBST and incubated in DAB (0.2 mg/ml PBS; 0.03% H_2O_2) for 15 minutes. To stop the reaction, sections were rinsed in DW, after which they were dried and mounted by Entellan® new (Merck Millipore).

Whole-mount *in situ* hybridization

Whole-mount in situ hybridization analyses were performed as previously described (Hojo et al., 2007). cDNAs used as the templates for the probes of marker genes were isolated from the d-rR strain by RT-PCR, except *pax2* (kindly provided by Wittblodt laboratory (Koster et al., 1997)). The partial fragments of *eya-1*, *dlx3b*, *bmp4*, *stm-l* and *sparc* were amplified by using following specific primers (5' to 3'): *eya-1*, CAGGAGAGTACAGTACCATCCACA and CCTGTCCGAGCCCTGGCGGCTGCA (Hochmann et al., 2007) ; *pax2*, GCIGAYCCITTYWSIGCIATGCA and GGRTTISWRAAICKCCAIGCYTCRTTRTA, (Koster et al., 1997) ; *dlx3b*, GGGATCCATGAGCGCCGGACAGACC and GCTCGAGATAAACAGCTCCCACGCTCT (Hochmann et al., 2007); *bmp4*,

TGCTCTATTTTCTGTCGAGACATC and GTTGTGTGGAGTCTGATTAAGGTG; *starmaker-like*, GCGAGGAATTGGATTCAGCAGATGA and GCCTGGCAAGGCAAACAAACAGGAA (Bajoghli et al., 2009) ; *sparc*, AGGGGGAGTTTGAGCACATC and AGGGATCAGCACCATTTCTG (Nemoto et al., 2008). For the expression analyses of *olpks*, cDNAs used as the templates for the probes were amplified by RT-PCR from the d-rR strain at st. 22. The full length of *olpks* was isolated by using following specific primers (5' to 3'): ATGGAGGACGGAATAGCCGTGG and TTAGCTGCTGCTGTGGACAAACTCC.

For histological analysis, whole-mount *in situ* hybridization samples were embedded in Technovit 8100 resin (Heraues-Kulzer) and sliced into 5-7 μm-thick sections.

Transmitted electron microscopy

Embryos were fixed with 2% PFA and 2% glutaraldehyde buffered in 0.1 M cacodylate buffer and postfixed in 2% OsO_4 in 0.1 M cacodylate buffer. Uranyl acetate and lead stain solution were used for contrast enhancement. The specimens were embedded in Quetol-812. Ultrathin sections (70 nm) were analyzed and documented with an electron microscope (JEOL, JEM-1400 Plus).

Genetic mapping

Positional cloning of the *ha* locus was carried out as previously described (Kimura et al., 2004). Mapping was performed by using EST markers and information from the Medaka genome database (UT-genome browser: http://medaka.utgenome.org/).

RT-PCR

RT-PCR analysis of *olpks* was performed using total RNA from embryos, fry and adult tissues. cDNA libraries were generated using the SuperScript First-Strand Synthesis System III for RT-PCR (Invitrogen). The primers 5'-CAAGTGTTGCAGCCAATAGAATTTC-3' and 5'-CTCCTGCCACCCTCCCGTGAGGCCCT-3' were used to amplify a 780 bp fragment of *olpks*. In addition, following primers were used to amplify expected 896 bp and 1047 bp fragments of *olpks-2* (LOC101169644: XP_004081384) and *olpks-3* (LOC101170716: XP_004080917), respectively (5' to 3'): *olpks-2*, GAAACAAACGCCGCACACATGCATC and CTTTGCTGGCATCTCATCGCTCTTT; *olpks-3*, CAGATTTGACTTAGCGGGCTGGTAT and GAACTGAGAGATCAAAGACGTCACCT.

Morpholino knockdown and mRNA rescue in medaka embryos

The morpholino antisense oligonucleotide (MOs; Gene Tools LLC) for the first-Met of OlPKS was as follows: 5'-AACCACGGCTATTCCGTCCTCCATG-3'. *in vitro* syntheses of mRNAs were conducted as reported previously (Yokoi et al., 2007). Full length of *olpks* was isolated from the d-rR strain by RT-PCR. The sequences of primers are described in 'Whole-mount *in situ* hybridization'. For injection of *olpks* mRNA with active site mutation, *ki79* fish was used because it likely carries a null mutation. Amino acid of the active site in each enzymatic domain was substituted as follows (with nucleotide sequences): KS, 173Cys→Asn (TGC→AAC); AT, 608Ser→Ala (TCC→GCA); DH, 914His→Ala (CAC→GCC); KR, 1859Tyr→Phe (TAC→TTC); ACP, 2010Ser→Ala (TCC→GCC); Loop (interdomain region; negative control), 435Thr→Ala (ACC→GCC) (Reid et al., 2003; Smith et al., 2003; Witkowski et al., 1996). Microinjection of MO or mRNAs was carried out as previously described (Yokoi et al., 2007).

Generation of the *ha* chimeric medaka

Transplantation experiments were performed based on the previous works (Shimada et al., 2008). [Tg (β-actin:DsRed)] were used as *wt* donors, whereas *ha* fish were prepared as hosts. At the morula stage, both the donors and hosts were dechorionated by hatching liquid. At the mid-blastula stage, the embryos were placed on V-shaped grooves of a 1.5% agarose gel immersed in Yamamoto's Ringer solution (the Ringer's solution for medaka), and then

the cells were transplanted to the prospective head area of the embryo, using a micromanipulator (Narishige, M-152) in combination with a microinjector (Narishige, IM-6).

After incubating these embryos overnight, we discarded the embryos whose ear region was largely occupied by *wt* cells. The presence or absence of otoliths and the number of fluorescent cells were assessed by observations around st. 29 using a confocal fluorescence microscope (Zeiss, LSM710). To evaluate how many *wt* cells were contained in the epithelium of the chimeric embryo, I calculated the ratio of area of the red labeled cells to all epithelial cells in a single plane of confocal images. For each OV, I select a plane where *wt* (red) cells are most abundant. ImageJ software was used for measuring the areas of transplanted cells (http://rsbweb.nih.gov/ij/). For the control experiment, *ha* fish ubiquitously expressing DsRed were obtained: [Tg (β-actin:DsRed)] and *ha* medaka were mated, and F_1 fish expressing DsRed were crossed with each other, followed by F_2 screening for *ha* phenotypes. Using this [$ha^{-/-}$; Tg (β-actin:DsRed)] animals as the donors, transplantation experiments were conducted by the same way.

OlPKS expression in *A. oryzae* and medaka rescue assay

The entire OlPKS ORF was amplified and subcloned into a fungal expression vector,

pTAex3. The resulting expression plasmid pTA-*olpks* was used for transformation of *A. oryzae* M-2-3 according to the protoplast-PEG method described by Gomi *et al.* (Gomi et al., 1987). They were subcultured in minimal medium (Czapek-Dox) plate. The pTA-*olpks* transformans were inoculated into 10 mL preculture medium (carbon source: glucose 20 g/L) in a 50 mL tube (Falcon) and cultured at 30°C for 3 days on a rotary shaker (150 rpm). Each 10 ml of the seed culture was inoculated into 1 L of induction medium (carbon source: starch 20g/L) for 4 days using the same cultural conditions. The mycelia from 1 L culture collected by filtration were added acetone (2 L) and stirred for 1 hour at room temperature to extract polyketide-derivatives. The acetone extract was filtered and the filtrate was concentrated to small volume to remove acetone. The residue (200 ml) was moved to a 2 L separating funnel and added 1 L H_2O and 0.5 L ethyl acetate to partition between ethylacete/H_2O (x 2). The ethyl acetate (upper) layer (1 L) was concentrated to dryness to give a colorless oil (approx. 0.5 g). The oil was next partitioned between hexane (200 ml)/90% methanol (200 ml), and 90% methanol layer (lower layer) was collected and concentrated to dryness to give the material (approx. 0.2 g) for medaka assay. The material was re-dissolved in a small amount of DMSO (approx. 1 ml) for the medaka assay. I prepared the negative control from a transformant with the empty pTAex3 vector.

Each extract re-dissolved in DMSO was diluted in 1:10-1:5 with Yamamoto's

Ringer solution. The chorions of *ha* embryos, stage of st. 21, were gently polished with a sandpaper to remove the attaching filaments, and incubated with the solution overnight. After brief washing by Yamamoto's Ringer solution, embryos were cultured in normal Yamamoto's Ringer solution another night until evaluation. At around st. 29, I evaluated whether one otic vesicle had otoliths (either 1 or 2 otoliths in the otic vesicle) or didn't have otolith at all.

Purification of OlPKS protein expressed in *A. oryzae* transformant

A transformant expressing OlPKS was cultivated as described above and mycelium was collected and frozen. Mycelium was ground in a frozen mortar by a pestle and suspended in buffer A (50 mM KH_2PO_4 [pH 7.5], 150 mM NaCl, 10% glycerol, 1 mM Tris [2-carboxyethyl]phosphine and Complete EDTA-free protease inhibitor cocktail (Roche)). The mixture was stirred at 4°C for 15 min and subsequently centrifuged (12,000 g, 15 minutes). The supernatant was filtered through Miracloth (Calbiochem). Ni-NTA superflow (Qiagen) was added to the supernatant, and the solution was stirred at 4°C for 1 hour. The protein/resin mixture was loaded into a gravity flow column, and proteins were purified with a gradient of imidazole in buffer A. The purified histidine-tagged protein was dialyzed against buffer A.

Western blotting for purified OlPKS

Western blotting was performed as previously described with some modifications (Matsuo et al., 2013). Purified OlPKS protein was mixed with 2x SDS buffer and shaken at 37°C. After separation by 7.5% polyacrylamide gels, gels were transferred onto polyvinylidene difluoride membranes (Millipore) by semidry-blotting with three buffers (recommended by Atto (Atto, AE-1460 EzBlot)). Anti-OlPKS serum was used for primary antibody (dilution is 1:20,000).

Genomic research

Animal type I PKS sequences were retrieved by TBLASTN against genome sequences of each species or BLASTP search against nr-protein database using the OlPKS sequence as a query. TBLASTN parameters: default settings at NCBI TBLASTN, except [Word size = 2] and [No Filter against low complexity regions]. For each candidate, domain search was done by Pfam sequence search, and then assessed for the presence of an animal-FAS homologous sequence and the constitution of domains; the basic domains for type I PKS, KS and AT, as well as additional domains (*i.e.*, DH, KR, ACP etc.).

Phylogenetic analysis

To draw the molecular phylogenetic tree, I used three groups of *pks* related genes; animal type I PKSs (listed in Table 4), animal FASs and non-animal PKSs. We searched for animal FASs using BLASTP against the genome database of major model animals and some species that have non-FAS PKS. The complete amino acid sequence of human FAS (NP_004095) was used as the query to retrieve animal FASs. Additionally, we thoroughly searched each group of non-animal organisms (*e.g.*, plants, fungi and bacteria) for sequences similar to OlPKS (full length amino acid sequence) by conducting individual BLASTP searches against each group independently. Some type II PKSs were used as outgroups. Multiple sequence alignment was performed using CLUSTAL W and the Maximum parsimony phylogenetic tree was constructed using the RAxML web service (Stamatakis et al., 2008) and NJ plot program. As previously reported (Castoe et al., 2007; Kroken et al., 2003), I conducted phylogenetic analyses using KS domain (approx. 400 amino acid length), the most conserved domain of type I PKS.

Cloning of sea urchin *pks* genes

Two *pks* genes have been reported for a sea urchin *Strongylocentrotus purpuratus*, *sppks-1* (XM_788471 (Calestani et al., 2003)) and *sppks-2* (NM_001252084 (Beeble and Calestani,

2012)). Based on these sequences, primers were designed for the amplification of *H. pulcherrimus pks* genes. Mixed embryonic cDNA (gastrula, prism and pluteus stages) was used as the template for amplification using ExTaq (TaKaRa). The partial fragments of *hppks-1* (1146 nt) and *hppks-2* (1219 nt) were isolated by using following specific primers, respectively (5' to 3'): CCTGTTTTCTAATCAGTGCTTG and ACRGATCCAATCTTGAGAGG, GATCGCTAACGCTCAACCAT and GTACCWGTACCATGYGCTTC.

Whole mount *in situ* hybridization for sea urchin embryos

Sea urchin (*Hemicentrotus pulcherrimus*) gametes were collected from adults and fertilized. Embryos were cultured in sea water until sampling. Embryos and larvae were fixed in 4% paraformaldehyde. Whole mount *in situ* hybridization was performed according to Arenas-Mena et al. (Arenas-Mena et al., 2000) with a slight modification, using a different blocking buffer (0.1 M Tris-Cl (pH7.5), 0.15 M NaCl, 0.5% Blocking Reagent (Roche)) for anti-DIG antibody incubation. Riboprobes containing digoxigenin-UTP were synthesized by standard methods. Antisense and sense (control) probes were made for partial sequences of *hppks-1* or *hppks-2*.

Morpholino knockdown in sea urchin embryos

Microinjection of MOs was carried out as described previously with some modifications (Katow et al., 2014). MOs (Gene Tools LLC) for first-Met blocking and their five-mispair controls were as follows (small letters in control sequences indicate substituted nucleotides).

hppks-1: 5'-CTGGTTTTATTGCTTCCCATGTTGA-3', *hppks-2*: 5'-CCCTCCAACTATCTTCCATAACTCA-3', *hppks-1* control: 5'-CTGcTaTTATTcCTTCCgATcTTGA -3', *hppks-2* control: 5'-CCgTgCAAgTATgTTCgATAACTCA-3'.

References

Addadi, L., Weiner, S., 1985. Interactions between acidic proteins and crystals: stereochemical requirements in biomineralization. Proc. Natl. Acad. Sci. U S A 82, 4110-4114.

Ageenko, N.V., Kiselev, K.V., Odintsova, N.A., 2011. Expression of Pigment Cell-Specific Genes in the Ontogenesis of the Sea Urchin Strongylocentrotus intermedius. Evid Based Complement Alternat Med 2011, 730356.

Anderson, H.C., 1969. Vesicles associated with calcification in the matrix of epiphyseal cartilage. The Journal of cell biology 41, 59-72.

Arenas-Mena, C., Cameron, A.R., Davidson, E.H., 2000. Spatial expression of Hox cluster genes in the ontogeny of a sea urchin. Development (Cambridge, England) 127, 4631-4643.

Awakawa, T., Yokota, K., Funa, N., Doi, F., Mori, N., Watanabe, H., Horinouchi, S., 2009. Physically discrete beta-lactamase-type thioesterase catalyzes product release in atrochrysone synthesis by iterative type I polyketide synthase. Chemistry & biology 16, 613-623.

Bajoghli, B., Ramialison, M., Aghaallaei, N., Czerny, T., Wittbrodt, J., 2009. Identification of starmaker-like in medaka as a putative target gene of Pax2 in the otic vesicle. Developmental dynamics : an official publication of the American Association of Anatomists 238, 2860-2866.

Beeble, A., Calestani, C., 2012. Expression pattern of polyketide synthase-2 during sea urchin development. Gene Expr Patterns 12, 7-10.

Beniash, E., Addadi, L., Weiner, S., 1999. Cellular control over spicule formation in sea urchin embryos: A structural approach. J Struct Biol 125, 50-62.

Borelli, G., Mayer-Gostan, N., De Pontual, H., Boeuf, G., Payan, P., 2001. Biochemical relationships between endolymph and otolith matrix in the trout (Oncorhynchus mykiss) and turbot (Psetta maxima). Calcified tissue international 69, 356-364.

Boskey, A.L., 1989. Hydroxyapatite Formation in a Dynamic Collagen Gel System: Effects of Type I Collagen, Lipids, and Proteoglycans. J Phys Chem 93, 1628-1633.

Boskey, A.L., Posner, A.S., 1977. In vitro nucleation of hydroxyapatite by a bone calcium-phospholipid-phosphate complex. Calcif Tissue Res 22 Suppl, 197-201.

Calestani, C., Rast, J.P., Davidson, E.H., 2003. Isolation of pigment cell specific genes in the sea urchin embryo by differential macroarray screening. Development (Cambridge, England) 130, 4587-4596.

Campana, S.E., 1999. Chemistry and composition of fish otoliths: pathway, mechanisms and applications. Mar. Ecol. Prog. Ser. 188, 263-297.

Castoe, T.A., Stephens, T., Noonan, B.P., Calestani, C., 2007. A novel group of type I polyketide synthases (PKS) in animals and the complex phylogenomics of PKSs. Gene 392, 47-58.

Chen, J., Thomas, H.F., Jin, H., Jiang, H., Sodek, J., 1996. Expression of rat bone sialoprotein

promoter in transgenic mice. Journal of bone and mineral research : the official journal of the American Society for Bone and Mineral Research 11, 654-664.

Clendenon, S.G., Shah, B., Miller, C.A., Schmeisser, G., Walter, A., Gattone, V.H., 2nd, Barald, K.F., Liu, Q., Marrs, J.A., 2009. Cadherin-11 controls otolith assembly: evidence for extracellular cadherin activity. Developmental dynamics : an official publication of the American Association of Anatomists 238, 1909-1922.

Colantonio, J.R., Vermot, J., Wu, D., Langenbacher, A.D., Fraser, S., Chen, J.N., Hill, K.L., 2009. The dynein regulatory complex is required for ciliary motility and otolith biogenesis in the inner ear. Nature 457, 205-209.

Cox, R.J., Simpson, T.J., 2009. Fungal type I polyketide synthases. Methods in enzymology 459, 49-78.

Della Sala, G., Hochmuth, T., Costantino, V., Teta, R., Gerwick, W., Gerwick, L., Piel, J., Mangoni, A., 2013. Polyketide genes in the marine sponge Plakortis simplex: a new group of mono-modular type I polyketide synthases from sponge symbionts. Environmental microbiology reports 5, 809-818.

Dey, A., Bomans, P.H., Muller, F.A., Will, J., Frederik, P.M., de With, G., Sommerdijk, N.A., 2010. The role of prenucleation clusters in surface-induced calcium phosphate crystallization. Nature materials 9, 1010-1014.

Foerstner, K.U., Doerks, T., Creevey, C.J., Doerks, A., Bork, P., 2008. A computational screen for type I polyketide synthases in metagenomics shotgun data. PloS one 3, e3515.

Fujii, I., Watanabe, A., Sankawa, U., Ebizuka, Y., 2001. Identification of Claisen cyclase domain in fungal polyketide synthase WA, a naphthopyrone synthase of Aspergillus nidulans. Chemistry & biology 8, 189-197.

Fukuda, I., Ooki, S., Fujita, T., Murayama, E., Nagasawa, H., Isa, Y., Watanabe, T., 2003. Molecular cloning of a cDNA encoding a soluble protein in the coral exoskeleton. Biochemical and biophysical research communications 304, 11-17.

Gebauer, D., Volkel, A., Colfen, H., 2008. Stable prenucleation calcium carbonate clusters. Science (New York, N.Y 322, 1819-1822.

Gomi, K., Iimura, Y., Hara, S., 1987. Integrative Transformation of Aspergillus oryzae with a Plasmid Containing the Aspergillus nidulans argB Gene. Agric Biol Chem 51, 2549-2555.

Haddon, C., Lewis, J., 1996. Early ear development in the embryo of the zebrafish, Danio rerio. The Journal of comparative neurology 365, 113-128.

Hochmann, S., Aghaallaei, N., Bajoghli, B., Soroldoni, D., Carl, M., Czerny, T., 2007. Expression of marker genes during early ear development in medaka. Gene Expr Patterns 7, 355-362.

Hojo, M., Takashima, S., Kobayashi, D., Sumeragi, A., Shimada, A., Tsukahara, T., Yokoi, H., Narita, T., Jindo, T., Kage, T., Kitagawa, T., Kimura, T., Sekimizu, K., Miyake, A., Setiamarga,

D., Murakami, R., Tsuda, S., Ooki, S., Kakihara, K., Naruse, K., Takeda, H., 2007. Right-elevated expression of charon is regulated by fluid flow in medaka Kupffer's vesicle. Development, growth & differentiation 49, 395-405.

Hopwood, D.A., 1997. Genetic Contributions to Understanding Polyketide Synthases. Chem Rev 97, 2465-2498.

Horinouchi, S., 2009. Combinatorial biosynthesis of plant medicinal polyketides by microorganisms. Current opinion in chemical biology 13, 197-204.

Hughes, I., Thalmann, I., Thalmann, R., Ornitz, D.M., 2006. Mixing model systems: using zebrafish and mouse inner ear mutants and other organ systems to unravel the mystery of otoconial development. Brain research 1091, 58-74.

Hunter, G.K., Goldberg, H.A., 1993. Nucleation of hydroxyapatite by bone sialoprotein. Proceedings of the National Academy of Sciences of the United States of America 90, 8562-8565.

Hunter, G.K., Wong, K.S., Kim, J.J., 1988. Binding of calcium to glycosaminoglycans: an equilibrium dialysis study. Arch Biochem Biophys 260, 161-167.

Ijiri, K., 2000. Vestibular and visual contribution to fish behavior under microgravity. Adv. Space Res. 25, 1997-2006.

Inoue, H., Ohira, T., Nagasawa, H., 2007. Significance of the N- and C-terminal regions of CAP-1, a cuticle calcification-associated peptide from the exoskeleton of the crayfish, for calcification. Peptides 28, 566-573.

Inoue, H., Ohira, T., Ozaki, N., Nagasawa, H., 2004. A novel calcium-binding peptide from the cuticle of the crayfish, Procambarus clarkii. Biochemical and biophysical research communications 318, 649-654.

Inoue, H., Ozaki, N., Nagasawa, H., 2001. Purification and structural determination of a phosphorylated peptide with anti-calcification and chitin-binding activities in the exoskeleton of the crayfish, Procambarus clarkii. Bioscience, biotechnology, and biochemistry 65, 1840-1848.

Jain, M., Cox, J.S., 2005. Interaction between Polyketide Synthase and Transporter Suggests Coupled Synthesis and Export of Virulence Lipid in M. tuberculosis PLOS pathogens. 1, 12-19.

Jenke-Kodama, H., Sandmann, A., Muller, R., Dittmann, E., 2005. Evolutionary implications of bacterial polyketide synthases. Molecular biology and evolution 22, 2027-2039.

John, U., Beszteri, B., Derelle, E., Van de Peer, Y., Read, B., Moreau, H., Cembella, A., 2008. Novel Insights into Evolution of Protistan Polyketide Synthases through Phylogenomic Analysis. Protist 159, 21-30.

Jones, B.M., Edwards, R.J., Skipp, P.J., O'Connor, C.D., Iglesias-Rodriguez, M.D., 2011. Shotgun proteomic analysis of Emiliania huxleyi, a marine phytoplankton species of major biogeochemical importance. Marine biotechnology 13, 496-504.

Kamura, K., Kobayashi, D., Uehara, Y., Koshida, S., Iijima, N., Kudo, A., Yokoyama, T., Takeda,

H., 2011. Pkd1l1 complexes with Pkd2 on motile cilia and functions to establish the left-right axis. Development (Cambridge, England) 138, 1121-1129.

Kashchiev, D., 2000. Theory and Basic Aplications. Butterworth-Heinemann.

Kasugai, S., Nagata, T., Sodek, J., 1992. Temporal studies on the tissue compartmentalization of bone sialoprotein (BSP), osteopontin (OPN), and SPARC protein during bone formation in vitro. J Cell Physiol 152, 467-477.

Katow, H., Katow, T., Abe, K., Ooka, S., Kiyomoto, M., Hamanaka, G., 2014. Mesomere-derived glutamate decarboxylase-expressing blastocoelar mesenchyme cells of sea urchin larvae. Biology open 3, 94-102.

Kimura, T., Jindo, T., Narita, T., Naruse, K., Kobayashi, D., Shin, I.T., Kitagawa, T., Sakaguchi, T., Mitani, H., Shima, A., Kohara, Y., Takeda, H., 2004. Large-scale isolation of ESTs from medaka embryos and its application to medaka developmental genetics. Mechanisms of development 121, 915-932.

Koster, R., Stick, R., Loosli, F., Wittbrodt, J., 1997. Medaka spalt acts as a target gene of hedgehog signaling. Development (Cambridge, England) 124, 3147-3156.

Kozubek, A., Tyman, J.H., 1999. Resorcinolic Lipids, the Natural Non-isoprenoid Phenolic Amphiphiles and Their Biological Activity. Chem Rev 99, 1-26.

Kroken, S., Glass, N.L., Taylor, J.W., Yoder, O.C., Turgeon, B.G., 2003. Phylogenomic analysis of type I polyketide synthase genes in pathogenic and saprobic ascomycetes. Proceedings of the National Academy of Sciences of the United States of America 100, 15670-15675.

Leibundgut, M., Maier, T., Jenni, S., Ban, N., 2008. The multienzyme architecture of eukaryotic fatty acid synthases. Current opinion in structural biology 18, 714-725.

Lowenstam, H.A., Weiner, S., 1989. On Biomineralization. Oxford Univ. Press, Oxford.

Lowenstein, O., 1971. The labyrinth, in: Hoar, W.S., Randall, D.J. (Eds.), Fish Physiology. Academic Press NY, pp. 207-240.

Ma, S.M., Li, J.W., Choi, J.W., Zhou, H., Lee, K.K., Moorthie, V.A., Xie, X., Kealey, J.T., Da Silva, N.A., Vederas, J.C., Tang, Y., 2009. Complete reconstitution of a highly reducing iterative polyketide synthase. Science (New York, N.Y 326, 589-592.

Mann, K., Wilt, F.H., Poustka, A.J., 2010. Proteomic analysis of sea urchin (Strongylocentrotus purpuratus) spicule matrix. Proteome Sci 8, 33.

Marsh, M.E., Chang, D.K., King, G.C., 1992. Isolation and characterization of a novel acidic polysaccharide containing tartrate and glyoxylate residues from the mineralized scales of a unicellular coccolithophorid alga Pleurochrysis carterae. The Journal of biological chemistry 267, 20507-20512.

Matsuo, M., Shimada, A., Koshida, S., Saga, Y., Takeda, H., 2013. The establishment of rotational polarity in the airway and ependymal cilia: analysis with a novel cilium motility

mutant mouse. Am J Physiol Lung Cell Mol Physiol 304, 736-745.

Merolli, A., Bosetti, M., Giannotta, L., Lloyd, A.W., Denyer, S.P., Rhys-Williams, W., Love, W.G., Gabbi, C., Cacchioli, A., Leali, P.T., Cannas, M., Santin, M., 2006. In vivo assessment of the osteointegrative potential of phosphatidylserine-based coatings. J Mater Sci Mater Med 17, 789-794.

Miyabe, K., Tokunaga, H., Endo, H., Inoue, H., Suzuki, M., Tsutsui, N., Yokoo, N., Kogure, T., Nagasawa, H., 2012. GSP-37, a novel goldfish scale matrix protein: identification, localization and functional analysis. Faraday Discuss 153, 463-481.

Mizuno, R., Ijiri, K., 2003. Otolith formation in a mutant medaka with a deficiency in gravity-sensing. Adv. Space Res. 32, 1513-1520.

Murayama, E., Herbomel, P., Kawakami, A., Takeda, H., Nagasawa, H., 2005. Otolith matrix proteins OMP-1 and Otolin-1 are necessary for normal otolith growth and their correct anchoring onto the sensory maculae. Mechanisms of development 122, 791-803.

Murayama, E., Okuno, A., Ohira, T., Takagi, Y., Nagasawa, H., 2000. Molecular cloning and expression of an otolith matrix protein cDNA from the rainbow trout, Oncorhynchus mykiss. Comparative biochemistry and physiology. Part B, Biochemistry & molecular biology 126, 511-520.

Murayama, E., Takagi, Y., Nagasawa, H., 2004. Immunohistochemical localization of two otolith matrix proteins in the otolith and inner ear of the rainbow trout, Oncorhynchus mykiss: comparative aspects between the adult inner ear and embryonic otocysts. Histochem Cell Biol 121, 155-166.

Murayama, E., Takagi, Y., Ohira, T., Davis, J.G., Greene, M.I., Nagasawa, H., 2002. Fish otolith contains a unique structural protein, otolin-1. Eur J Biochem 269, 688-696.

Nagasawa, H., 2013. The molecular mechanism of calcification in aquatic organisms. Bioscience, biotechnology, and biochemistry 77, 1991-1996.

Nemoto, Y., Chatani, M., Inohaya, K., Hiraki, Y., Kudo, A., 2008. Expression of marker genes during otolith development in medaka. Gene Expr Patterns 8, 92-95.

Nikolouli, K., Mossialos, D., 2012. Bioactive compounds synthesized by non-ribosomal peptide synthetases and type-I polyketide synthases discovered through genome-mining and metagenomics. Biotechnol. Lett. 34, 1393-1403.

Noro, S., Yamamoto, N., Ishikawa, Y., Ito, H., Ijiri, K., 2007. Studies on the morphology of the inner ear and semicircular canal endorgan projections of ha, a medaka behavior mutant. Fish Biol J Medaka 11, 31-41.

O'Brien, R.V., Davis, R.W., Khosla, C., Hillenmeyer, M.E., 2014. Computational identification and analysis of orphan assembly-line polyketide synthases. The Journal of antibiotics 67, 89-97.

Ohtsuka, M., Kikuchi, N., Yokoi, H., Kinoshita, M., Wakamatsu, Y., Ozato, K., Takeda, H., Inoko,

H., Kimura, M., 2004. Possible roles of zic1 and zic4, identified within the medaka Double anal fin (Da) locus, in dorsoventral patterning of the trunk-tail region (related to phenotypes of the Da mutant). Mechanisms of development 121, 873-882.

Omran, H., Kobayashi, D., Olbrich, H., Tsukahara, T., Loges, N.T., Hagiwara, H., Zhang, Q., Leblond, G., O'Toole, E., Hara, C., Mizuno, H., Kawano, H., Fliegauf, M., Yagi, T., Koshida, S., Miyawaki, A., Zentgraf, H., Seithe, H., Reinhardt, R., Watanabe, Y., Kamiya, R., Mitchell, D.R., Takeda, H., 2008. Ktu/PF13 is required for cytoplasmic pre-assembly of axonemal dyneins. Nature 456, 611-616.

Payan, P., Kossmann, H., Watrin, A., Mayer-Gostan, N., Boeuf, G., 1997. Ionic composition of endolymph in teleosts: origin and importance of endolymph alkalinity. The Journal of experimental biology 200, 1905-1912.

Pisam, M., Jammet, C., Laurent, D., 2002. First steps of otolith formation of the zebrafish: role of glycogen? Cell and tissue research 310, 163-168.

Pouget, E.M., Bomans, P.H., Goos, J.A., Frederik, P.M., de With, G., Sommerdijk, N.A., 2009. The initial stages of template-controlled CaCO3 formation revealed by cryo-TEM. Science (New York, N.Y 323, 1455-1458.

Rafiq, K., Cheers, M.S., Ettensohn, C.A., 2012. The genomic regulatory control of skeletal morphogenesis in the sea urchin. Development (Cambridge, England) 139, 579-590.

Riley, B.B., Zhu, C., Janetopoulos, C., Aufderheide, K.J., 1997. A critical period of ear development controlled by distinct populations of ciliated cells in the zebrafish. Developmental biology 191, 191-201.

Sarikaya, M., Tamerler, C., Jen, A.K., Schulten, K., Baneyx, F., 2003. Molecular biomimetics: nanotechnology through biology. Nature materials 2, 577-585.

Sato, A., Nagasaka, S., Furihata, K., Nagata, S., Arai, I., Saruwatari, K., Kogure, T., Sakuda, S., Nagasawa, H., 2011. Glycolytic intermediates induce amorphous calcium carbonate formation in crustaceans. Nature chemical biology 7, 197-199.

Satsangi, A., Satsangi, N., Glover, R., Satsangi, R.K., Ong, J.L., 2003. Osteoblast response to phospholipid modified titanium surface. Biomaterials 24, 4585-4589.

Schibler, A., Malicki, J., 2007. A screen for genetic defects of the zebrafish ear. Mech. Dev. 124, 592-604.

Service, M., Wardlaw, A.C., 1984. Echinochrome-A as a bactericidal substance in the coelomic fluid of Echinus esculentus. Comp Biochem Physiol B 79, 161-165.

Shimada, A., Yabusaki, M., Niwa, H., Yokoi, H., Hatta, K., Kobayashi, D., Takeda, H., 2008. Maternal-zygotic medaka mutants for fgfr1 reveal its essential role in the migration of the axial mesoderm but not the lateral mesoderm. Development (Cambridge, England) 135, 281-290.

Smith, S., Tsai, S.C., 2007. The type I fatty acid and polyketide synthases: a tale of two

megasynthases. Natural product reports 24, 1041-1072.

Sollner, C., Burghammer, M., Busch-Nentwich, E., Berger, J., Schwarz, H., Riekel, C., Nicolson, T., 2003. Control of crystal size and lattice formation by starmaker in otolith biomineralization. Science (New York, N.Y 302, 282-286.

Sollner, C., Schwarz, H., Geisler, R., Nicolson, T., 2004. Mutated otopetrin 1 affects the genesis of otoliths and the localization of Starmaker in zebrafish. Development genes and evolution 214, 582-590.

Squires, T.M., Weidman, M.S., Hain, T.C., Stone, H.A., 2004. A mathematical model for top-shelf vertigo: the role of sedimenting otoconia in BPPV. Journal of biomechanics 37, 1137-1146.

Stamatakis, A., Hoover, P., Rougemont, J., 2008. A rapid bootstrap algorithm for the RAxML Web servers. Systematic biology 57, 758-771.

Staunton, J., Weissman, K.J., 2001. Polyketide biosynthesis: a millennium review. Natural product reports 18, 380-416.

Stooke-Vaughan, G.A., Huang, P., Hammond, K.L., Schier, A.F., Whitfield, T.T., 2012. The role of hair cells, cilia and ciliary motility in otolith formation in the zebrafish otic vesicle. Development (Cambridge, England) 139, 1777-1787.

Straight, P.D., Fischbach, M.A., Walsh, C.T., Rudner, D.Z., Kolter, R., 2007. A singular enzymatic megacomplex from Bacillus subtilis. Proc. Natl. Acad. Sci. U S A 104, 305-310.

Sunagawa, I., 2003. Crystals: Growth, Morphology, and Perfection. Cambridge University Press.

Suzuki, M., Saruwatari, K., Kogure, T., Yamamoto, Y., Nishimura, T., Kato, T., Nagasawa, H., 2009. An acidic matrix protein, Pif, is a key macromolecule for nacre formation. Science (New York, N.Y 325, 1388-1390.

Takagi, Y., Takahashi, A., 1999. Characterization of ootolith soluble-matrix producing cells in the saccular epithelium of rainbow trout (Oncorhynchus mykiss) inner ear. Anat Rec 254, 322-329.

Takeda, H., Shimada, A., 2010. The art of medaka genetics and genomics: what makes them so unique? Annu Rev Genet 44, 217-241.

Tohse, H., Ando, H., Mugiya, Y., 2004. Biochemical properties and immunohistochemical localization of carbonic anhydrase in the sacculus of the inner ear in the salmon Oncorhynchus masou. Comparative biochemistry and physiology 137, 87-94.

Tohse, H., Mugiya, Y., 2001. Effects of enzyme and anion transport inhibitors on in vitro incorporation of inorganic carbon and calcium into endolymph and otoliths in salmon Oncorhynchus masou. Comparative biochemistry and physiology 128, 177-184.

Tohse, H., Saruwatari, K., Kogure, T., Nagasawa, H., Takagi, Y., 2009. Control of Polymorphism and Morphology of Calcium Carbonate Crystals by a Matrix Protein Aggregate in Fish Otoliths.

Cryst. Growth Des. 9, 4897-4901.

Tomita, H., 1990. Strains and mutants. Biology of the Medaka (Egami., N. ed. University of Tokyo Press), 111-127.

Van, C., P., 2003. Biomineralization and Global Biogeochemical Cycles. Rev. Mineral. Geochem. 54, 357-381.

Weiner, S., Addadi, L., 1991. Acidic macromolecules of mineralized tissues: the controllers of crystal formation. Trends Biochem Sci 16, 252-256.

Weiner, S., Hood, L., 1975. Soluble protein of the organic matrix of mollusk shells: a potential template for shell formation. Science (New York, N.Y 190, 987-989.

Westbroek, P., Brown, C.W., Van Bleijswijk, J., Brownlee, C., Brummer, G.J., Conte, M., Egge, J., Fernandez, E., Jordan, R., Knappertsbusch, M., Stefels, J., Veldhuis, M., Van der Wal, P., Young, J., 1993. A model system approach to biological climate forcing. The example of Emiliania huxleyi. Global. Planet. Change. 8, 27-46.

Whitfield, T.T., Granato, M., van Eeden, F.J., Schach, U., Brand, M., Furutani-Seiki, M., Haffter, P., Hammerschmidt, M., Heisenberg, C.P., Jiang, Y.J., Kane, D.A., Kelsh, R.N., Mullins, M.C., Odenthal, J., Nusslein-Volhard, C., 1996. Mutations affecting development of the zebrafish inner ear and lateral line. Development (Cambridge, England) 123, 241-254.

Wu, D., Freund, J.B., Fraser, S.E., Vermot, J., 2011. Mechanistic basis of otolith formation during teleost inner ear development. Developmental cell 20, 271-278.

Wuthier, R.E., 1975. Lipid composition of isolated epiphyseal cartilage cells, membranes and matrix vesicles. Biochim Biophys Acta 409, 128-143.

Yamane, H., Takayama, M., Sunami, K., Sakamoto, H., Imoto, T., Anniko, M., 2010. Blockage of reuniting duct in Meniere's disease. Acta Otolaryngol 130, 233-239.

Acknowledgements

First of all, I would like to express my gratitude to my mentor Professor Hiroyuki Takeda for his guidance, encouragement and patience.

I would also like to express my sincere appreciation to Drs. Yasuo Ohnishi, Yohei Katsuyama and Kazutoshi Shindo for helpful discussion and experimental support on biochemical experiments using *A.oryzae*.; to the members of Ohnishi Laboratory, past and present, particularly Ms. Adeline Muliandi, Dr. Takayuki Hayashi and Dr. Takuya Makino; to Drs. Masato Kiyomoto, Gen Hamanaka and Mariko Kondo for their providing the experimental data of sea urchin; to Drs. Ai Omi and Takanori Narita for their contributions to cloning of OlPKS and phenotypic analyses; to Dr. Atsuko Shimada and Mrs. Sayaka Tayama for their contributions to medaka chimeric analysis; to Dr. Naoki Irie for providing helpful suggestion about molecular phylogenic analyses; to Mrs. Yasuko Ozawa for excellent fish care.

I thank to Dr. Hiromichi Nagasawa for providing the anti-OmOMP1 serum; to Dr. Akira Kudo for providing the medaka mutant strain *ki79*; to Dr. Joachim Wittbrodt for providing the cDNA of *pax2*.

I thank to my supervisors and co-workers in Tokyo Metropolitan Government, Bureau of Waterworks and Institute of Public Health, for helping attend the university.

I am grateful to the members of Takeda Laboratory, past and present, for all they have done for my life in the laboratory. Particularly, I would like to express my appreciation to Drs. Tatsuya Tsukahara and Keiichiro Kamura for giving helpful suggestions and encouragement.

Finally, I am greatly indebted to my family for their heartfelt support, without which I would not have accomplished this study.